The LCLAT1/LYCAT acyltransferase is required for EGF-mediated phosphatidylinositol-3,4,5-trisphosphate generation and Akt signaling

Victoria Chan[a,b], Cristina Camardi[a,b], Kai Zhang[b], Laura A. Orofiamma[a,b], Karen E. Anderson[c], Jafarul Hoque[b], Leslie N. Bone[a,b], Yasmin Awadeh[a,b], Daniel K. C. Lee[d], Norman J. Fu[d], Jonathan T. S. Chow[d], Leonardo Salmena[d], Len R. Stephens[c], Phillip T. Hawkins[c], Costin N. Antonescu[a,b,*], and Roberto J. Botelho[a,b,*]

[a]Molecular Science Graduate Program, and [b]Department of Chemistry and Biology, Toronto Metropolitan University, Toronto, Ontario M5B2K3, Canada; [c]Signalling Programme, Babraham Institute, Cambridge CB22 4AT, United Kingdom; [d]Department of Pharmacology & Toxicology, University of Toronto, Toronto, Ontario M5S1A8, Canada

ABSTRACT **Receptor tyrosine kinases such as EGF receptor (EGFR) stimulate phosphoinositide 3 kinases to convert phosphatidylinositol-4,5-bisphosophate [PtdIns(4,5)P_2] into phosphatidylinositol-3,4,5-trisphosphate [PtdIns(3,4,5)P_3]. PtdIns(3,4,5)P_3 then remodels actin and gene expression, and boosts cell survival and proliferation. PtdIns(3,4,5)P_3 partly achieves these functions by triggering activation of the kinase Akt, which phosphorylates targets like Tsc2 and GSK3β. Consequently, unchecked upregulation of PtdIns(3,4,5)P_3-Akt signaling promotes tumor progression. Interestingly, 50–70% of PtdIns and PtdInsPs have stearate and arachidonate at *sn*-1 and *sn*-2 positions of glycerol, respectively, forming a species known as 38:4-PtdIns/PtdInsPs. LCLAT1 and MBOAT7 acyltransferases partly enrich PtdIns in this acyl format. We previously showed that disruption of LCLAT1 lowered PtdIns(4,5)P_2 levels and perturbed endocytosis and endocytic trafficking. However, the role of LCLAT1 in receptor tyrosine kinase and PtdIns(3,4,5)P_3 signaling was not explored. Here, we show that LCLAT1 silencing in MDA-MB-231 and ARPE-19 cells abated the levels of PtdIns(3,4,5)P_3 in response to EGF signaling. Importantly, LCLAT1-silenced cells were also impaired for EGF-driven and insulin-driven Akt activation and downstream signaling. Thus, our work provides first evidence that the LCLAT1 acyltransferase is required for receptor tyrosine kinase signaling.**

SIGNIFICANCE STATEMENT

- The function and regulation of enzymes like the LCLAT1 acyltransferase, which controls the unique acyl profile of phosphatidylinositol and phosphoinositides, are not well understood.
- The authors reveal that LCLAT1 is required for receptor tyrosine kinase signalling because without LCLAT1, EGFR and insulin fail to promote PI3K-Akt signalling.
- Given the dearth of drugs targeting LCLAT1, the results suggest that LCLAT1 is a novel target for drug discovery to manipulate phosphoinositide signalling.

Monitoring Editor
Alexander Sorkin
University of Pittsburgh Medical School

Received: Oct 11, 2023
Revised: Jul 2, 2024
Accepted: Jul 10, 2024

New Hypothesis

This article was published online ahead of print in MBoC in Press (http://www.molbiolcell.org/cgi/doi/10.1091/mbc.E23-09-0361) on July 18, 2024.

*Address correspondence to: Costin N. Antonescu (cantonescu@torontomu.ca); Roberto J. Botelho (rbotelho@torontomu.ca).

Abbreviations: BSA, bovine serum albumin; EGF, epidermal growth factor; EGFR, epidermal growth factor receptor; IP_3, inositol-1,4,5-trisphosphate; ER, endoplasmic reticulum; PtdIns, phosphatidylinositol; PtdIns(3)P, phosphatidylinositol-3-phosphate; PtdIns(4,5)P_2, phosphatidylinositol-4,5-bisphosphate; PtdIns(3,4,5)P_3, phosphatidylinositol-3,4,5-trisphosphate; PtdInsP, phosphoinositide; TIRF, total internal reflection fluorescence; TNBC, triple-negative breast cancer.

INTRODUCTION

Phosphoinositide (PtdInsP) lipid signaling orchestrates a variety of cellular functions such as organelle identity and membrane trafficking, ion channel activity, cytoskeletal organization, regulation of gene expression, modulation of metabolic activity, and cell proliferation and survival (Balla, 2013; Idevall-Hagren and De Camilli, 2015; Choy *et al.*, 2017; Dickson and Hille, 2019; Doumane *et al.*, 2022; Posor *et al.*, 2022). PtdInsPs are generated by the reversible phosphorylation of the phosphatidylinositol (PtdIns) headgroup by several types of lipid kinases and phosphatases. Collectively, and based on the headgroup phosphorylation, these enzymes can generate up to seven species of PtdInsPs (Balla, 2013; Choy *et al.*, 2017; Dickson and Hille, 2019; Posor *et al.*, 2022). Nonetheless, there is another facet of PtdInsP biology that is poorly defined at the regulatory and functional levels—the control and function of the acyl composition of PtdInsPs (D'Souza and Epand, 2014; Choy *et al.*, 2017; Traynor-Kaplan *et al.*, 2017; Barneda *et al.*, 2019; Bozelli and Epand, 2019).

In many mammalian tissues and cells, 50–70% of PtdIns and PtdInsPs are enriched for stearate and arachidonate at the *sn*-1 and *sn*-2 positions, respectively—this acyl combination is referred to as 38:4-PtdIns or 38:4-PtdInsPs (Milne *et al.*, 2005; Haag *et al.*, 2012; Imae *et al.*, 2012; Lee *et al.*, 2012; Anderson *et al.*, 2013; D'Souza and Epand, 2014; Anderson *et al.*, 2016; Traynor-Kaplan *et al.*, 2017; Barneda *et al.*, 2019). Additionally, this acyl composition is unique to PtdIns and PtdInsPs since other phospholipids have distinct acyl profiles (Hicks *et al.*, 2006; Traynor-Kaplan *et al.*, 2017; Barneda *et al.*, 2019; Bozelli and Epand, 2019). This suggests that the acyl groups of PtdIns and PtdInsPs do more than simply embedding the lipids into the membrane bilayer (Choy *et al.*, 2017; Barneda *et al.*, 2019; Bozelli and Epand, 2019). However, the exact acyl profile of PtdIns and PtdInsPs can vary between cell types, environmental conditions, and pathophysiological conditions such as cancer (Hicks *et al.*, 2006; Imae *et al.*, 2012; Anderson *et al.*, 2016; Traynor-Kaplan *et al.*, 2017; Mujalli *et al.*, 2018; Barneda *et al.*, 2019; Bozelli and Epand, 2019). For example, $p53^{-/-}$ cancer cells, prostate cancer cells and triple-negative breast cancer (TNBC) cells all have distinct acyl profiles of PtdIns relative to normal tissue (Naguib *et al.*, 2015; Rueda-Rincon *et al.*, 2015; Koizumi *et al.*, 2019; Freyr Eiriksson *et al.*, 2020). Yet, there is much to be understood about the regulatory mechanisms that establish and remodel the acyl profile of PtdIns and PtdInsPs, and their functional implications.

The LCLAT1 acyltransferase has been identified as one of the enzymes that remodels and enriches PtdIns and/or PtdInsPs in stearate at the *sn*-1 position (Imae *et al.*, 2012; D'Souza and Epand, 2014; Bone *et al.*, 2017; Zhang *et al.*, 2023). LCLAT1 is an ER-localized protein and is thought to act during the Lands' Cycle or PtdIns Cycle to enrich PtdIns in stearate at *sn*-1 (Imae *et al.*, 2012; Bone *et al.*, 2017; Barneda *et al.*, 2019; Blunsom and Cockcroft, 2020). Murine tissues deleted for LCLAT1 had reduced levels of 38:4-PtdIns, mono-PtdInsP, and bis-phosphorylated PtdInsPs (Imae *et al.*, 2012). More recently, we observed that LCLAT1 silencing reduced the relative levels of endosomal phosphatidylinositol-3-phosphate [PtdIns(3)P] and phosphatidylinositol-4,5-bisphosphate [PtdIns(4,5)P_2] on the plasma membrane, while the levels of phosphatidylinositol-4-phosphate [PtdIns(4)P] remained unchanged (Bone *et al.*, 2017). Importantly, PtdIns and bis-phosphorylated PtdInsPs (mostly PtdIns(4,5)P_2), but not monophosphorylated PtdInsPs (mostly PtdIns(4)P] were altered in their acyl profile upon LCLAT1 silencing. This effect on specific pools of PtdInsPs has also been observed in cells disrupted for LPIAT1/MBOAT7, an acyltransferase thought to enrich PtdIns/PtdInsPs in arachidonic acid (Anderson *et al.*, 2013).

PtdIns(4,5)P_2 regulates a number of functions including endocytosis, ion transport, and the cytoskeleton organization (Balla, 2013; Sun *et al.*, 2013; Katan and Cockcroft, 2020). PtdIns(4,5)P_2 is also a precursor for other signaling intermediates regulated by growth factor receptors like the EGF and its receptor, the EGF receptor (EGFR), a major receptor tyrosine kinase (Katan and Cockcroft, 2020; Orofiamma *et al.*, 2022). EGF binds and dimerizes EGFR, leading to receptor autophosphorylation on various tyrosine residues on the receptor's C-terminal tail region (Gullick *et al.*, 1985; Böni-Schnetzler and Pilch, 1987; Honegger *et al.*, 1987; Yarden and Schlessinger, 1987; Koland and Cerione, 1988; Linggi and Carpenter, 2006). Motifs harboring these phosphotyrosines serve as docking sites for adaptor proteins like Grb2, which assemble a signaling complex composed of other protein kinases and phosphatases, and lipid-metabolizing enzymes (Margolis *et al.*, 1990a; Holgado-Madruga *et al.*, 1996, 2; Rodrigues *et al.*, 2000; Orofiamma *et al.*, 2022). For example, active EGFR recruits and activates phospholipase Cγ (PLCγ), which hydrolyses PtdIns(4,5)P_2 into diacylglycerol and inositol-1,4,5-trisphosphate (IP_3), and which releases Ca^{2+} from endoplasmic reticulum stores (Santos *et al.*, 2017; Margolis *et al.*, 1990a; Margolis *et al.*, 1990b). In addition, Gab1, recruited to the membrane via interactions with EGFR-bound Grb2, engages class I phosphoinositide 3 kinases (PI3Ks) to convert PtdIns(4,5)P_2 to PtdIns(3,4,5)P_3 (Rodrigues *et al.*, 2000; Kiyatkin *et al.*, 2006). This burst of PtdIns(3,4,5)P_3 then recruits and activates PDK1 and Akt protein kinases (Alessi *et al.*, 1997; Stokoe *et al.*, 1997; Bellacosa *et al.*, 1998; Manning and Toker, 2017). Akt is a major driver of cell metabolism and growth by phosphorylating numerous targets like GSK3β and TSC2 (Cross *et al.*, 1995; Inoki *et al.*, 2002; Manning and Toker, 2017; Rodgers *et al.*, 2017; Sugiyama *et al.*, 2019). For example, Akt inactivates TSC2, a GTPase-activating protein (GAP) for the Rheb GTPase, thus promoting the mTORC1 pathway (Inoki *et al.*, 2002; Inoki *et al.*, 2003). The PtdIns(3,4,5)P_3-Akt-mTORC1 pathway is a major driver of cell growth, proliferation, survival, and differentiation (Dibble and Manning, 2013; Dey *et al.*, 2017; Manning and Toker, 2017; Sugiyama *et al.*, 2019). As a result, mutations that hyperactivate this pathway are often associated with human cancers like TNBC (Dey *et al.*, 2017; Li *et al.*, 2017).

Overall, given that LCLAT1 is a PI acyltransferase and the connection between EGF and PI3K-Akt pathway, we postulated that LCLAT1 disruption would impair EGF-mediated PtdIns(3,4,5)P_3-Akt signaling, reflecting a role for PI acyl profile specificity for signaling by this pathway. In fact, we found that LCLAT1 silencing in at least two cell lines impeded generation of PtdIns(3,4,5)P_3 and Akt activation upon addition of EGF.

RESULTS

LCLAT1 acyltransferase regulation of EGFR trafficking

In our previous work, LCLAT1 silencing altered the endocytosis and endosomal trafficking of the transferrin receptor in ARPE-19 cells (Bone *et al.*, 2017). We thus queried whether LCLAT1 disruption would alter the total and surface levels of EGFR and/or affect EGFR signaling in at least two human-derived cells lines: the noncancerous, male-derived ARPE-19 and the female-derived TNBC cell line, MDA-MB-231. To do this, we used previously designed and validated siRNA oligonucleotides against LCLAT1 (Bone *et al.*, 2017) and a nontargeting oligonucleotide (see *Materials and Methods*), transiently transfected cells twice, and after 48 h, we lysed the cells and probed for LCLAT1 levels by Western blotting. As shown in Figure 1A and Figure 2A respectively, control ARPE-19 and MDA-MB-231 cells displayed a major band at 35 kDa. After transfection

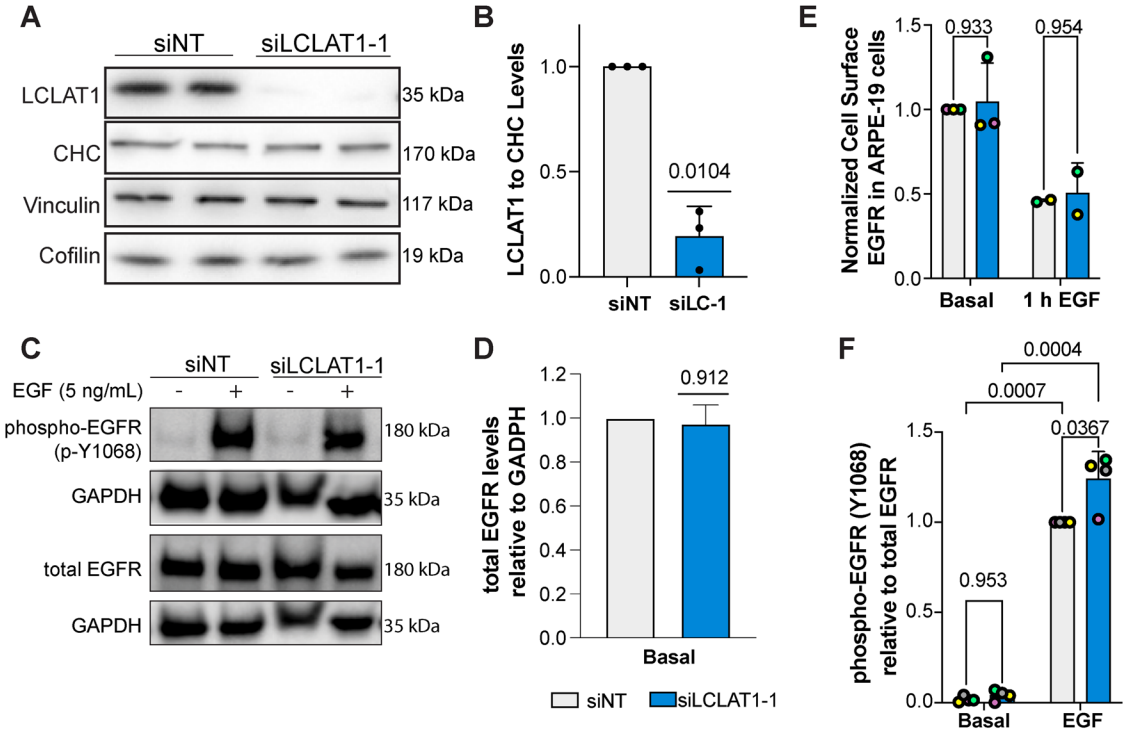

FIGURE 1: LCLAT1 silencing has no negative impact on EGFR activation, EGFR total levels, and EGFR surface levels in ARPE-19 cells. (A) Western blots showing repressed LCLAT1 expression in ARPE-19 cells transfected with siLCLAT1-1 oligonucleotides relative to nontargeting control siRNA (NT siRNA). Two replicate lanes per condition are shown. Clathrin heavy chain (CHC), cofilin, and vinculin were used as loading controls. (B) Normalized ratio of LCLAT1 expression to CHC in ARPE-19 cells. (C) ARPE-19 cells silenced for LCLAT1 or treated with nontargeting oligonucleotide were serum-starved and then stimulated with 5 ng/ml EGF for 5 min. Lysates were then probed for total EGFR or phospho-EGFR. GAPDH was employed as the loading control. (D) Quantification of total EGFR relative to the respective GAPDH signal. (E) Normalized cell surface EGFR detected by immunofluorescence before and after 1 h stimulation with 100 ng/ml EGF in nontargeted and LCLAT1-silenced ARPE-19 cells. (F) Quantification of phospho-EGFR (p-Y1068) relative to the respective total EGFR signal. All experiments were repeated a minimum of three times except in E (EGF stimulation, $n = 2$). Data points from matching independent experiments are color coded. For B, D, and F shown is mean ± STD. Data in E are shown as mean ± SEM where at least 40–80 cells were scored per condition per experiment. Data in B and D were analyzed by a one-sample *t* test using hypothetical value of 1. For data in E and F, a repeated measures two-way ANOVA followed by Sidak's (E) or Tukey's (F) post-hoc test was used. *p* values are indicated.

with siLCLAT1-1, this band was reduced by ~70% intensity in both cell types, manifesting efficient LCLAT1 silencing (Figure 1, A and B and Figure 2, A and B). We also observed reduced LCLAT1 expression in ARPE-19 and MDA-MB-231 cells transfected with independent siRNA oligonucleotides against LCLAT1 (Supplemental Figure S1, A and B, S2, A and B, and S4).

We next examined the effects of LCLAT1 silencing on total and surface levels of EGFR in these cells. We observed that LCLAT1 silencing in ARPE-19 and MDA-MB-231 cells did not alter total EGFR levels as measured by Western blotting (Figures 1, C and D and 2, C and D) nor the EGFR surface levels as measured by immunofluorescence of unpermeabilized cells under basal conditions (Figures 1E and 2E). Moreover, the surface levels of EGFR after 1 h of 100 ng/ml EGF stimulation dropped by a similar extend in both control and LCLAT1-silenced ARPE-19 (Figure 1E) and MDA-MB-231 (Figure 2E). Importantly, LCLAT1-silencing did not impair EGF-mediated phosphorylation of Y1068 of EGFR in ARPE-19 cells (Figure 1, C and F) and MDA-MB-231 cells (Figure 2, C and F); in fact, EGFR phosphorylation at Y1068 appears elevated in LCLAT1-silenced cells (Figure 2F). Overall, these data suggest that the steady-state levels and trafficking of EGFR, and immediate response to EGF in ARPE-19 and MDA-MB-231 cells did not decline during LCLAT1 silencing.

LCLAT1 acyltransferase silencing reduces PtdIns(3,4,5)P_3 synthesis in response to EGF

We previously observed that ARPE-19 cells silenced for LCLAT1 had ~30% reduction in PtdIns(4,5)P_2 levels (Bone *et al.*, 2017). To determine whether this was recapitulated in MDA-MB-231 cells, we generated cells stably engineered for doxycycline-inducible eGFP-PLCδ-PH, a reporter for PtdIns(4,5)P_2 (Stauffer *et al.*, 1998). We then quantified the fluorescence ratio of eGFP-PLCδ-PH on the plasma membrane over cytosolic signal by using FM4-64FX to define the plasma membrane. Upon silencing of LCLAT1 in these cells, the eGFP-PLCδ-PH fluorescence ratio of plasma membrane to cytosol declined significantly relative to nonsilenced cells (Figure 3, A and B) suggesting that LCLAT1-silenced MDA-MB-231 cells also had less PtdIns(4,5)P_2.

Next, a key outcome of EGFR stimulation is the activation of PI3Ks to convert PtdIns(4,5)P_2 to PtdIns(3,4,5)P_3 (Hu *et al.*, 1992; Rodrigues *et al.*, 2000; Orofiamma *et al.*, 2022). To determine whether PtdIns(3,4,5)P_3 synthesis was affected in LCLAT1-disturbed cells, we transfected ARPE-19 and MDA-MB-231 cells with plasmids encoding Akt-PH-GFP, a biosensor for 3-phosphorylated PtdInsPs (Várnai and Balla, 1998). The recruitment of Akt-PH-GFP to the plasma membrane in response to EGF was then quantified using

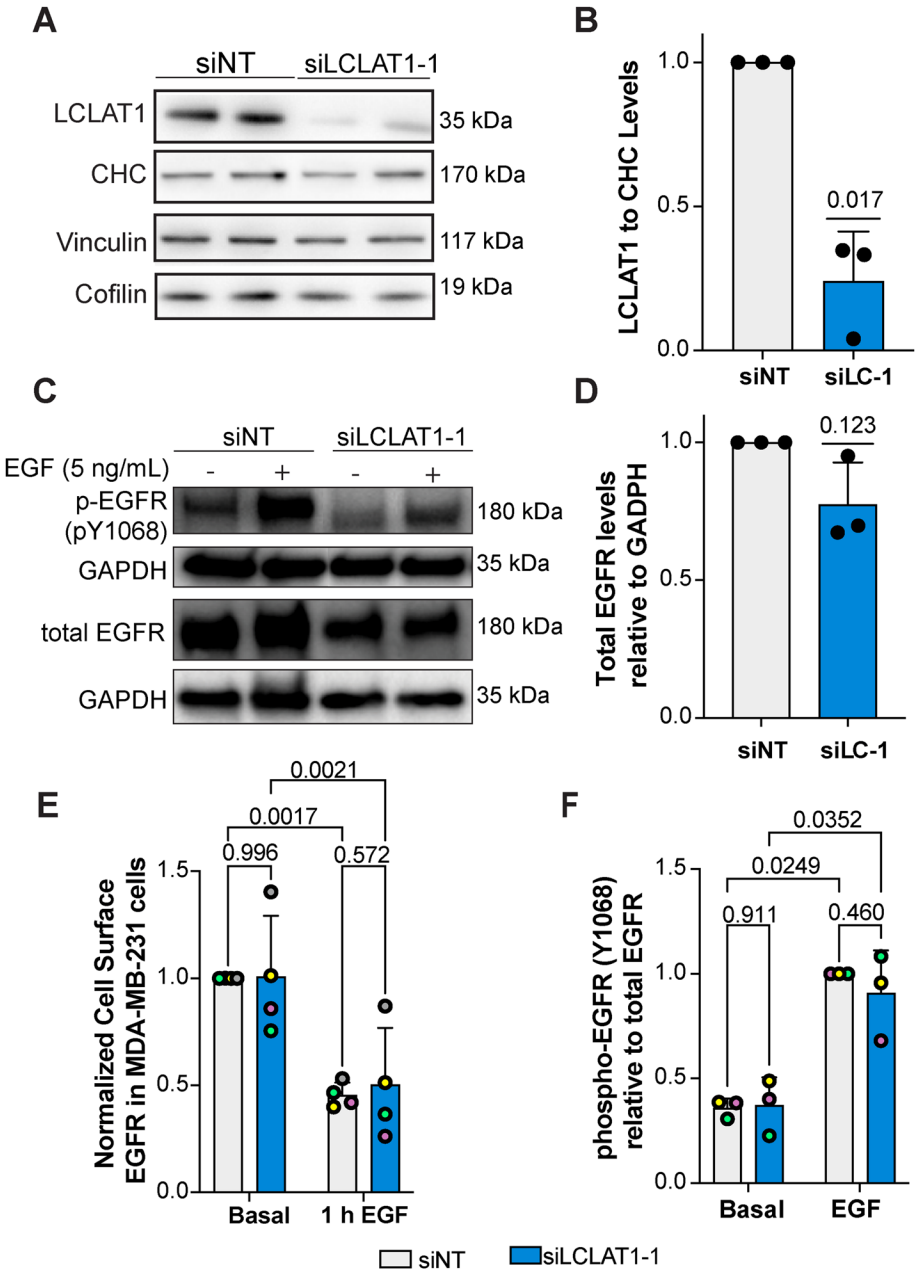

FIGURE 2: LCLAT1 silencing has no negative impact on EGFR activation, total EGFR levels, and surface EGFR levels in MDA-MB-231 cells. (A) Western blot showing LCLAT1 silencing in MDA-MB-231 cells transfected with siLCLAT1-1 (siLC-1) relative to nontargeting control siRNA (NT siRNA). Each condition shows two replicates. Clathrin heavy chain (CHC), vinculin, and cofilin were used as a loading control. (B) Normalized ratio of LCLAT1 expression to CHC signal in MDA-MB-231 cells. (C) MDA-MB-231 cells silenced for LCLAT1 or treated with nontargeting oligonucleotides were serum-starved and then stimulated with 5 ng/ml EGF for 5 min. Lysates were then probed for total EGFR or phospho-EGFR (pY-1068). GAPDH was employed as the loading control. (D) Quantification of total EGFR relative to respective GAPDH. (E) Normalized cell surface EGFR detected by immunofluorescence before and after 1 h stimulation with 100 ng/ml EGF in nontargeted and LCLAT1-silenced MDA-MB-231 cells. (F) Quantification of phospho-Y1068-EGFR relative to EGFR. All experiments were repeated at least three independent times. Data points from matching independent experiments are color coded. For B, D, and F, shown are the mean ± STD. For E, the mean ± SEM is shown where 50–100 cells were scored per condition per experiment. Data in B and D were analyzed by a one-sample *t* test using hypothetical value of 1. For data in E and F, a repeated measures two-way ANOVA followed by Tukey's post-hoc test was used. *p* values are shown.

two different methods. Given that ARPE-19 cells are exceptionally flat, we quantified the ratio of TIRF to epifluorescence fields (TIRF/Epi fluorescence ratio) as an indicator for PtdIns(3,4,5)P_3 levels at the plasma membrane. While control cells readily increased their Akt-PH-GFP on the plasma membrane after EGF stimulation, cells perturbed for LCLAT1 expression displayed substantially lower TIRF/Epifluorescence of their Akt-PH-GFP (Figure 3, C and D). We then assessed whether MDA-MB-231 cells were also impaired for PI3K signaling. Because these cells are rounder, we measured Akt-PH-GFP on the plasma membrane more readily in optical sections obtained from the middle of the cell by spinning disk confocal microscopy by sampling Akt-PH-GFP at the cell periphery against cytosolic signal. We tracked the Akt-PH-GFP recruitment over 10 min after adding EGF. We observed an increase in Akt-PH-GFP to the cell periphery after EGF stimulation of nonsilenced MDA-MB-231 cells (Figure 3, E and F). Importantly, this increase in Akt-PH-GFP at the cell periphery was suppressed in the LCLAT1-silenced cell group (Figure 3, E and F). Hence, despite near normal levels of EGFR and p-EGFR, we reveal that LCLAT1 expression is required for EGF-mediated increase in PI(3,4,5)P_3 levels in at least two cell types.

The impact of LCLAT1 acyltransferase expression on the acyl profile of PtdInsPs

We next examined the PtdInsP acyl profile and their relative levels by mass spectrometry in control (cells maintained in medium supplemented with serum), serum-starved (medium with no serum for 1 h and not further stimulated), and EGF-stimulated for 5 min. These conditions were examined in both ARPE-19 and MDA-MB-231 cells that were subjected to nontargeting siRNA or LCLAT1-silencing siRNA oligonucleotides. For this analysis, we normalized lipid spectral counts against synthetic standards added to the samples to generate a response ratio (see *Materials and Methods*). In addition, to correct for variation in cell input between experiments, we further normalized against an internal benchmark by comparing changes in 38:4 PtdIns, *mono*-PtdInsPs, *bis*-PtdInsPs, and PtdIns(3,4,5)P_3 relative to standardized 36:x-PtdIns and the corresponding 36:x-mono-PtdInsP and 36:xbis-PtdInsP since these species have previously been shown to be less affected by LCLAT1 expression relative to 38:4 species (Imae *et al.*, 2012; Bone *et al.*, 2017).

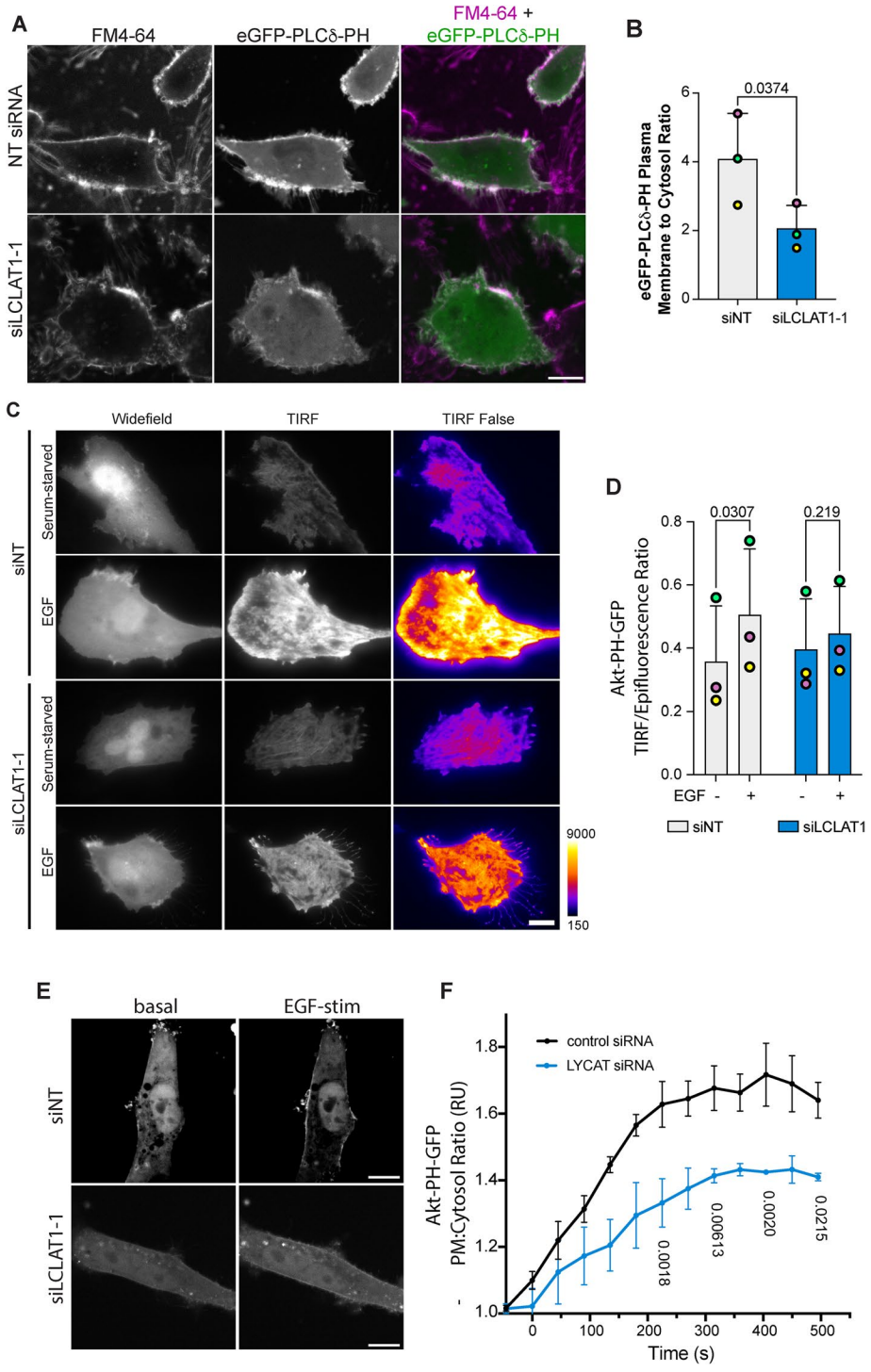

FIGURE 3: Defective PI(4,5)P_2 and EGF-stimulated PtdIns(3,4,5)P_3 synthesis in LCLAT1-silenced cells. MDA-MB-231 cells (A, E), and ARPE-19 (C) were mock-silenced or LCLAT1-silenced. (A) Confocal images of MDA-MB-231 cells stably expressing eGFP-PLCδ-PH (green) and labeled with FM4-46FX (magenta). (B) Quantification of eGFP-PLCδ-PH fluorescence on FM4-64X–labeled cell periphery relative to its cytosolic signal. (C) TIRF and epifluorescence microscopy of ARPE-19 cells mock-silenced or silenced for LCLAT1 and expressing Akt-PH-GFP. Cells were maintained serum starved or exposed to 20 ng/ml EGF for 5 min. The TIRF field is shown both in grayscale and as false-color (fire LUT), where black-indigo is weakest and yellow-white is strongest. For representation, cells selected expressed similar levels of Akt-PH-GFP. (D) Quantification of TIRF/epifluorescence ratio of Akt-PH-GFP. Total Akt-PH-GFP fluorescence in TIRF field is expressed as a ratio against the corresponding total fluorescence in the epifluorescence field. Shown is the ratio for serum-starved and EGF-stimulated control and LCLAT1-silenced cells. (E) Spinning disk confocal images of MDA-MB-231 cells mock-silenced or LCLAT1-silenced before and during 20 ng/ml EGF stimulation. (F) Quantification of Akt-PH-GFP fluorescence at the plasma membrane relative to its cytosolic signal from time-lapse imaging over 10 min of stimulation with 20 ng/ml EGF. Scale bar = 20 µm. All experiments were repeated three independent times. For B and D, data points from matching independent experiments are color coded. Shown is the mean ± SEM, where data in D were binned every 45 s (three images). For B and D, data are based on 30–50 transfected cells per condition per experiment. For F, a total of 23 transfected cells were traced over time over three independent experiments. Data in B were analyzed by paired Student *t* test. For D and F, repeated measures two-way ANOVA and Sidak's post-hoc test was used to test data in D. *p* values are shown.

We note that our previous normalization benchmark used the 38:x PtdInsP (not just 38:4) to its respective 36:x PtdInsP and an internal benchmark was not used (Bone *et al.*, 2017).

For ARPE-19 cells, the major acyl species of PtdIns, *mono*-, *bis*-, and *tris*-PtdInsP was 38:4, as expected. In fact, we only detected 38:4 acyl species for PtdIns(3,4,5)P_3. We then compared each group of 38:4 PtdInsPs with the 36:x-PtdIns and the corresponding 36:x-PtdInsP. Relative to 36:x-PtdIns, we saw that the levels of 38:4-PtdIns were reduced in LCLAT1-silenced cells (Figure 4A). In comparison, there was no significant difference in 38:4-*mono*-PtdInsPs relative to 36:x-PtdIns or 36:x-mono-PtdInsP in any treatment (Figure 4B; Supplemental Figure S3A). However, 38:4-*bis*-PtdInsPs declined in LCLAT1-silenced cells relative to 36:x-PtdIns (Figure 4C) and 36:x-bis-PtdInsPs (Supplemental Figure S3B). Lastly, EGF increased the levels of 38:4-PtdIns(3,4,5)P_3 relative to 36:x-PtdIns in both serum-starved nonsilenced and LCLAT1-silenced cells (Figure 4D). However, LCLAT1-silenced cells had a significant reduction in 38:4-PtdIns(3,4,5)P_3 levels relative to 36:x-PtdIns compared with nontargeted ARPE-19 cells (Figure 4D). We could not quantitatively compare 38:4-PtdIns(3,4,5)P_3 with 36:x-PtdIns(3,4,5)P_3 since we did not detect the latter. Overall, this suggests that 38:4-PtdIns(3,4,5)P_3 is the predominant acyl species of this phosphoinositide upon EGF stimulation and that LCLAT1 expression is required for its efficient synthesis. Overall, we reveal that ARPE-19 cells shift their acyl profile of PtdIns, *bis*-PtdInsPs, and PtdIns(3,4,5)P_3 upon LCLAT1-disruption, but not for *mono*-PtdInsPs.

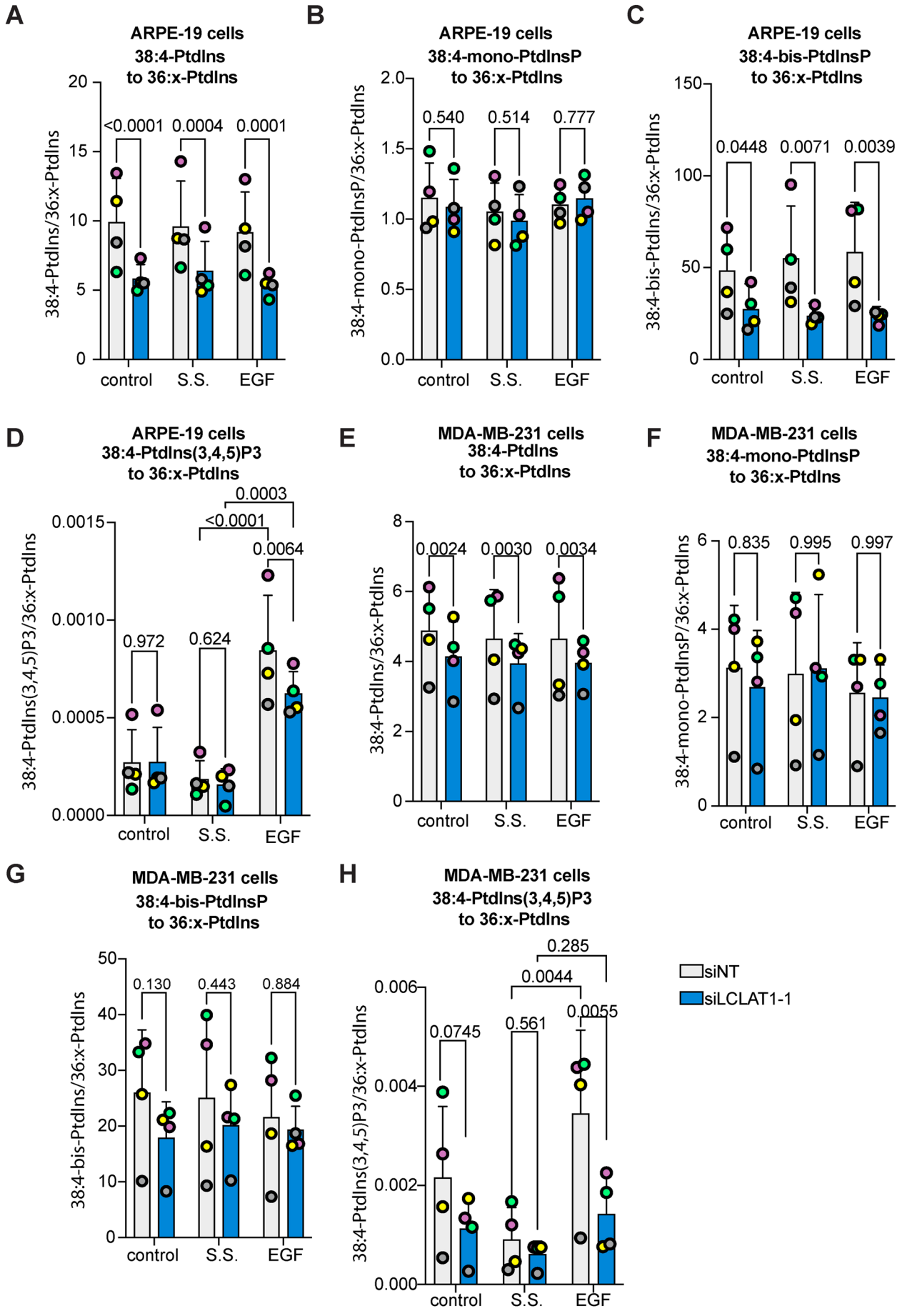
A
ARPE-19 cells
38:4-PtdIns
to 36:x-PtdIns
38:4-PtdIns/36:x-PtdIns
<0.0001
0.0004
0.0001
control
S.S.
EGF
B
ARPE-19 cells
38:4-mono-PtdInsP
to 36:x-PtdIns
38:4-mono-PtdInsP/36:x-PtdIns
0.540
0.514
0.777
C
ARPE-19 cells
38:4-bis-PtdInsP
to 36:x-PtdIns
38:4-bis-PtdIns/36:x-PtdIns
0.0448
0.0071
0.0039
D
ARPE-19 cells
38:4-PtdIns(3,4,5)P3
to 36:x-PtdIns
38:4-PtdIns(3,4,5)P3/36:x-PtdIns
0.0003
<0.0001
0.0064
0.972
0.624
E
MDA-MB-231 cells
38:4-PtdIns
to 36:x-PtdIns
38:4-PtdIns/36:x-PtdIns
0.0024
0.0030
0.0034
F
MDA-MB-231 cells
38:4-mono-PtdInsP
to 36:x-PtdIns
38:4-mono-PtdInsP/36:x-PtdIns
0.835
0.995
0.997
G
MDA-MB-231 cells
38:4-bis-PtdInsP
to 36:x-PtdIns
38:4-bis-PtdIns/36:x-PtdIns
0.130
0.443
0.884
H
MDA-MB-231 cells
38:4-PtdIns(3,4,5)P3
to 36:x-PtdIns
38:4-PtdIns(3,4,5)P3/36:x-PtdIns
0.285
0.0044
0.0055
0.561
0.0745
siNT
siLCLAT1-1

We similarly investigated the lipidomic profile of MDA-MB-231 cells. The major acyl species for all PtdInsPs and PtdIns was again 38:4 and we once again only detected 38:4-PtdIns(3,4,5)P_3 acyl species in our samples. LCLAT1 suppression lowered 38:4-PtdInsP relative to 36:x-PtdInsP in MDA-MB-231 cells, but unlike ARPE-19 cells, this change did not transfer to the *bis*-species (Figure 4G; Supplemental Figure S3D). Instead, resting cells had a significant difference in 38:4-*mono*-PtdInsPs relative to 36:x-*mono*-PtdInsPs (Supplemental Figure S3C), but not serum-starved or EGF or relative to 36:x-PtdIns (Figure 4F; Supplemental Figure S3C). Most striking, was the elevation in the ratio of 38:4-PtdIns(3,4,5)P_3 to 36:x-PtdInsP in nonsilenced MDA-MB-231 cells after EGF stimulation and relative to serum-starved cells (Figure 4H). Importantly, LCLAT1-perturbed MDA-MB-231 cells failed to significantly increase 38:4-PtdIns(3,4,5)P_3 ratio compared with 36:x-PtdIns after EGF stimulation (Figure 4H), suggesting that MDA-MB-231 cells were more sensitive to this than ARPE-19 cells. Overall, we propose that LCLAT1 expression is essential to support EGFR-dependent activation of PI3K signaling in at least two distinct cell lines, but the impact on acyl profile can vary between cell type, PtdInsP species, and treatments.

Akt activation by EGF is defective in LCLAT1-silenced cells

Because LCLAT1-silenced cells had lower EGF-induced PtdInsP(3,4,5)P_3 levels relative to nonsilenced counterparts, we next examined whether Akt activation was also impaired in ARPE-19 and MDA-MB-231 cells after EGF exposure. To do this, we probed for phosphorylation at S473 using an antibody that recognizes all isoforms of Akt when phosphorylated (pan-phospho-Akt antibody). Relative to serum-starved ARPE-19 and MDA-MB-231 cells, EGF caused a large increase in phospho-Akt in nonsilenced control cells (Figure 5, A and B and Figure 6, A and B). Importantly, both ARPE-19 and MDA-MB-231 cells silenced for LCLAT1 displayed substantially reduced phospho-Akt levels after EGF stimulation (Figure 5, A and B and Figure 6, A and B). We also observed impaired p-Akt levels in ARPE-19 cells (Supplemental Figure S1, A and C; Figure 5G) and MDA-MB-231 cells (Supplemental Figure S2, A and C) treated with independent oligonucleotides against LCLAT1. Because Akt1 has been reported to respond to PtdIns(3,4,5)P_3 while Akt2 to PtdIns(3,4)P_2 generated by SHIP2 from PtdIns(3,4,5)P_3 (Liu *et al.*, 2018), we sought to determine whether silencing LCLAT1 exhibited any isoform-specific effects on Akt phosphorylation that may reveal additional insights into PtdInsP perturbation in LCLAT1-silenced cells. We thus probed with anti-p-Akt1 (S473) and p-Akt2 (S474) antibodies to test this. We reveal that ARPE-19 and MDA-MB-231 silenced for LCLAT1 after EGF stimulation have lower levels of both p-Akt1 and p-Akt2 relative to their respective total Akt1 and Akt2 (Figure 5, C–F and Figure 6, C–F).

To evince whether LCLAT1 was important for Akt signaling by other receptors, we assessed insulin-mediated activation of Akt in MDA-MB-231 cells. As with EGF, LCLAT1 silencing hindered phosphorylation of Akt after insulin activation (Figure 6, G and H). Thus, LCLAT1 silencing negatively impacts Akt activation by both EGF and insulin signaling, implying that LCLAT1 may broadly support activation of PI3K-Akt signaling by receptor tyrosine kinases. Finally, we tested whether LCLAT1 silencing also perturbed the ERK pathway by EGFR. Here, we saw cell-type specific effects. In ARPE-19 cells, EGF stimulation of phospho-ERK1/2 was predominantly unperturbed by LCLAT1 suppression with two oligonucleotides (Figure 5, G and H). However, in MDA-MB-231 cells inhibited for LCLAT1 displayed suppression of ERK phosphorylation in response to EGF (Figure 6, E and F). Overall, LCLAT1 is required for Akt activation by receptor tyrosine kinases and may play a role in ERK stimulation in a context-dependent manner.

LCLAT1 acyltransferase silencing impairs Akt-mediated regulation of downstream targets

Because Akt activation is defective in LCLAT1-silenced cells after addition of EGF, we next examined whether this effect percolated to several known Akt targets. To test for specific targets, we measured the phosphorylation state of Tsc2 and GSK3β by Western blotting. In ARPE-19 and MDA-MB-231 cells transfected with a nontargeting oligonucleotide (control siRNA), EGF promoted robust phosphorylation of these specific Akt substrates (Figure 7). In contrast, LCLAT1 silencing led to a considerable decline in the EGF-induced phosphorylation of Tsc2 in ARPE-19 (Figure 7, A and B) and MDA-MB-231 (Figure 7, E and F) cells. For GSK3β, the effects were less clear—for ARPE-19 cells, there was a tendency for less phosphorylation of GSK3β (Figure 7, C and D), but this was not the case for MDA-MB-231 cells (Figure 7, G and H); neither cell line demonstrated a significant decrease in EGF-stimulated GSK3β phosphorylation upon LCLAT1 silencing. Overall, loss of LCLAT1 appears to compromise TSC2 regulation by Akt.

We also probed for the expression levels of cell cycle checkpoint proteins like Mdm2, p53, and p21 (Gordon *et al.*, 2018). In doing so, we observed that LCLAT1-1 oligonucleotide, but not LCLAT1-5, tended to deplete Mdm2 protein levels in both ARPE-19 (Supplemental Figure S4, A and B) and MDA-MB-231 cells (Supplemental Figure S4, E and F), despite similar levels of silencing of LCLAT1 by each LCLAT1 oligonucleotide. These oligonucleotides were significantly different from each other in their effect on p21 levels in ARPE-19 cells, with LCLAT1-1 trending upward (Supplemental Figure S4, A and C). There was no significant difference between oligonucleotides and nontargeting in their effect on p21 levels in MDA-MB-231 cells and for p53 protein levels in both cells (Supplemental Figure S4). Thus, given these differences in outcome of LCLAT1 oligonucleotides that may reflect kinetics of silencing or even some limited off-target effects by the LCLAT1-1 siRNA sequence, we advise caution when considering the LCLAT1-1 oligonucleotide in future experiments. Regardless, we emphasize that the effects on Akt signaling were consistent across all oligonucleotides and in both cell types.

FIGURE 4: Relative levels of 38:4 PtdIns and PtdInPs in ARPE-19 and MDA-MB-231 cells silenced for LCLAT1. ARPE-19 cells (A–D) and MBA-MB-231 cells (E–I) were mock-silenced (siNT) or LCLAT1-silenced. Cells were then grown in regular medium (control), serum-starved (ss), and stimulated with 5 ng/ml EGF for 5 min (EGF). Reactions were quenched and lipid extracted after addition of internal standards to primary cell extracts. PtdInsPs were measured by mass spectrometry (HPLC-MS). Shown is the ratio of standardized 38:4-PtdIns (A, E), 38:4-mono-PtdInsP (B, G), 38:4-bis-PtdInsP (C, H), and 38:4-PtdIns(3,4,5)P_3 (D, I) to the standardized sum of 36:1 and 36:2-PtdIns (referred to as 36:x-PtdIns). Lipid analysis was repeated four independent times. Data points from matching independent experiments are color coded. Shown are the mean ±STD. A repeated-measures, two-way ANOVA and Sidak's post-hoc (A–C, and E–G) and Tukey's post-hoc (D, H) tests were used to assess the data. *p* values are disclosed.

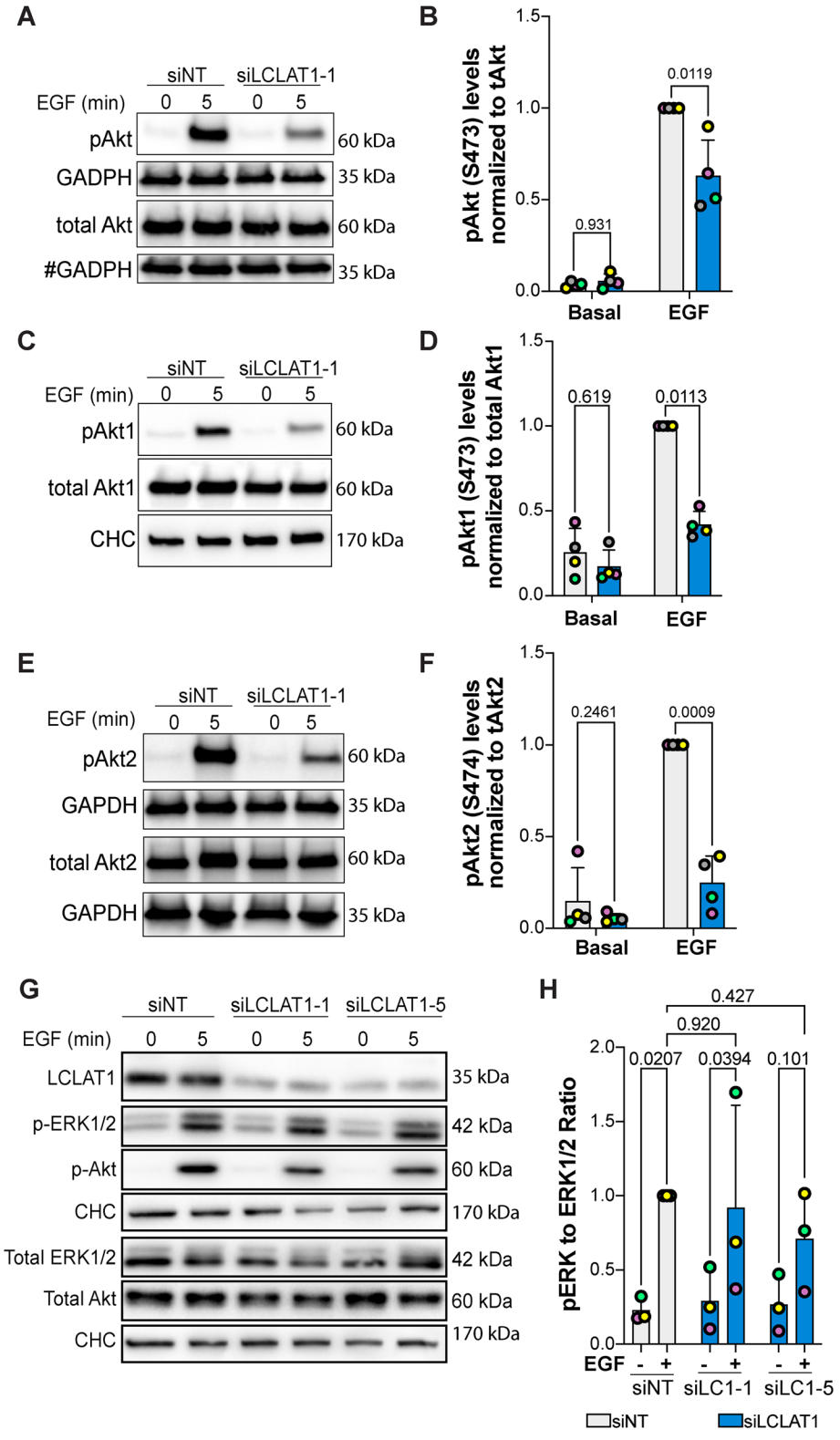

FIGURE 5: LCLAT1 is required for EGF-stimulated Akt activation in ARPE-19 cells. (A, C, E) Mock-silenced (siNT) and LCLAT1-silenced ARPE-19 cells were serum-starved (0 min) or stimulated with 5 ng/ml EGF for 5 min. Lysates were then prepared, separated by SDS–PAGE and probed by Western blotting for pan-phospho-Akt and total pan-Akt (A), phospho-Akt1 and total Akt1 (C), and phospho-Akt2 and total Akt2 (E). Clathrin heavy chain (CHC) or GAPDH were used as loading controls. # indicates that the GAPDH blot was also used as loading control for p-TSC2 in Figure 7G since they originated from the same membrane cut across to probe for different sized proteins. (B, D, F) Quantification of pan-pAkt (B), pAkt1 (D), and pAkt2 (F) normalized to respective total pan-Akt, Akt1, and Akt2. (G) ARPE-19 cells transfected with nontargeting, LCLAT1-1, or LCLAT1-5 oligonucleotides and stimulated as above. Lysates were probed with LCLAT1, phospho-ERK1/2, ERK1/2, phospho-Akt, Akt, and CHC as loading control for each blot. (E) Quantification of phospho-ERK1/2 relative to total ERK1/2. Mean ± STD are shown from $n = 4$ (A, C, and E) and $n = 3$ (G) independent experiments are shown. Data points from matching independent experiments are color coded. Repeated measures two-way ANOVA and Sidak's (B, D, F) or Tukey's (H) post-hoc tests were used to statistically test the data. p values are indicated.

DISCUSSION

Here, we reveal that the LCLAT1 acyltransferase is needed to promote EGFR-mediated PtdIns(3,4,5)P_3-Akt signaling in at least two cell lines. While EGFR levels and its early activation by EGF were unaffected, cells perturbed for LCLAT1 had reduced PtdIns(3,4,5)P_3 levels and diminished Akt activation. We thus identified an important role for the poorly studied LCLAT1 acyltransferase and highlighted this enzyme as part of a novel druggable lipid acyl profile remodeling pathway to modulate PI3K signaling.

The role of LCLAT1 in generating PtdIns(3,4,5)P_3

We provide at least three pieces of evidence that LCLAT1 is important to generate PtdIns(3,4,5)P_3 during EGF-mediated signaling. First, we revealed that LCLAT1-silenced MDA-MB-231 and ARPE-19 cells were impaired for the recruitment of the Akt-PH-GFP, a biosensor for PtdIns(3,4,5)P_3 levels (Haugh *et al.*, 2000; Marshall *et al.*, 2001), to the plasma membrane after EGF stimulation. Second, we observed that LCLAT1-silenced cells possessed lower relative levels of 38:4-PtdIns(3,4,5)P_3. Incidentally, 38:4-PtdIns(3,4,5)P_3 was the only observable acyl-based species for PtdIns(3,4,5)P_3 in both cell types, likely because the other acyl isoforms of PtdIns(3,4,5)P_3 were below the detection limit of our current analysis. Regardless, this is consistent with other studies examining the acyl profile of PtdIns(3,4,5)P_3, identifying 38:4 as the major species, though this can vary with tissue, cell type, and genetics (Clark *et al.*, 2011; Mujalli *et al.*, 2018; Koizumi *et al.*, 2019; Morioka *et al.*, 2022). Third, Akt activation was impaired in LCLAT1-silenced cells after EGF stimulation. Hence, collectively these varied approaches indicate that LCLAT1-silenced cells are defective in promoting PtdIns(3,4,5)P_3 levels, and possibly PtdIns(3,4)P_2.

A key question then is how does LCLAT1 contribute to PtdIns(3,4,5)P_3 synthesis. We

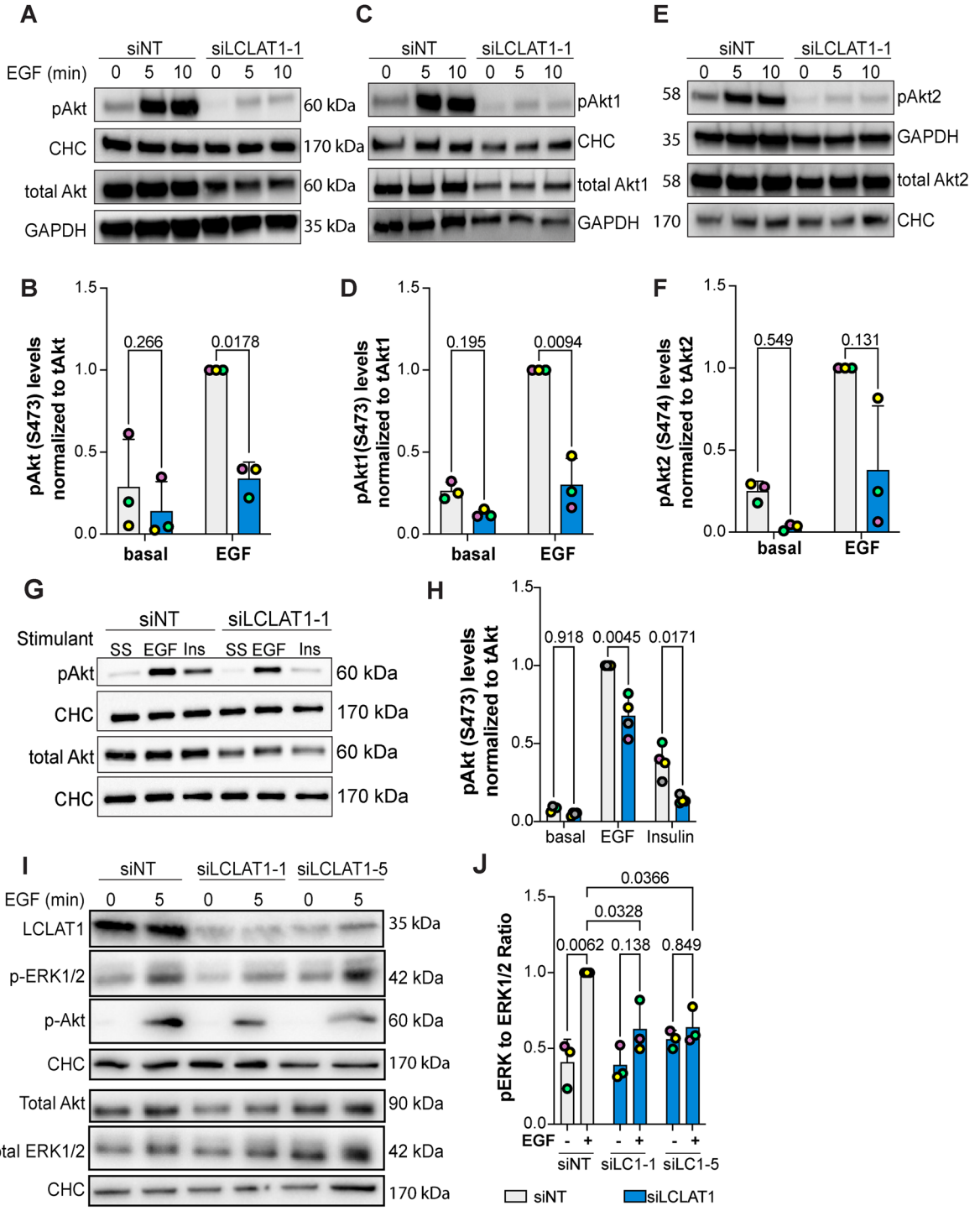

FIGURE 6: LCLAT1 is required for EGF-stimulated Akt activation in MDA-MB-231 cells. (A, C, E) Mock-silenced and LCLAT1-silenced MDA-MB-231 cells were serum-starved (0 min) or stimulated with 5 ng/ml EGF for 5 min or 10 min. Lysates were then prepared, separated by SDS–PAGE and probed by Western blotting for pan-phospho-Akt and total pan-Akt (A), phospho-Akt1 and total Akt1 (C), and phospho-Akt2 and total Akt2 (E). Clathrin heavy chain (CHC) or GAPDH were used as loading controls. (B, D, F) Quantification of pan-pAkt (B), pAkt1 (D), and pAkt2 (F) normalized to respective total pan-Akt, Akt1, and Akt2. (G) Western blotting of nonsilenced and LCLAT1-silenced cells after serum-starvation (SS), 5 ng/ml EGF, or 10 ng/ml insulin (Ins) stimulation for 5 min. Lysates were probed for pAkt, total Akt, and clathrin heavy chain. (E) Quantification of pAkt relative to total Akt in treatments described in G. (I) Western blot of MDA-MB-231 cells silenced for LCLAT1 with either LCLAT1-1 or LCLAT1-5 oligonucleotides. Cells were serum-starved or stimulated with 5 ng/ml EGF for 5 min. Lysates were probed with LCLAT1, phospho-ERK1/2, ERK1/2, phosphor-Akt, Akt, and corresponding CHC as loading control for each blot. (J) Quantification of phospho-ERK to total ERK. Shown are the mean ± STD from $n = 3–4$ independent experiments. Data points from matching independent experiments are color coded. Repeated measures two-way ANOVA and Sidak's (B, D, F) or Tukey's (H, J) post-hoc tests were used to statistically test the data. *p* values are displayed.

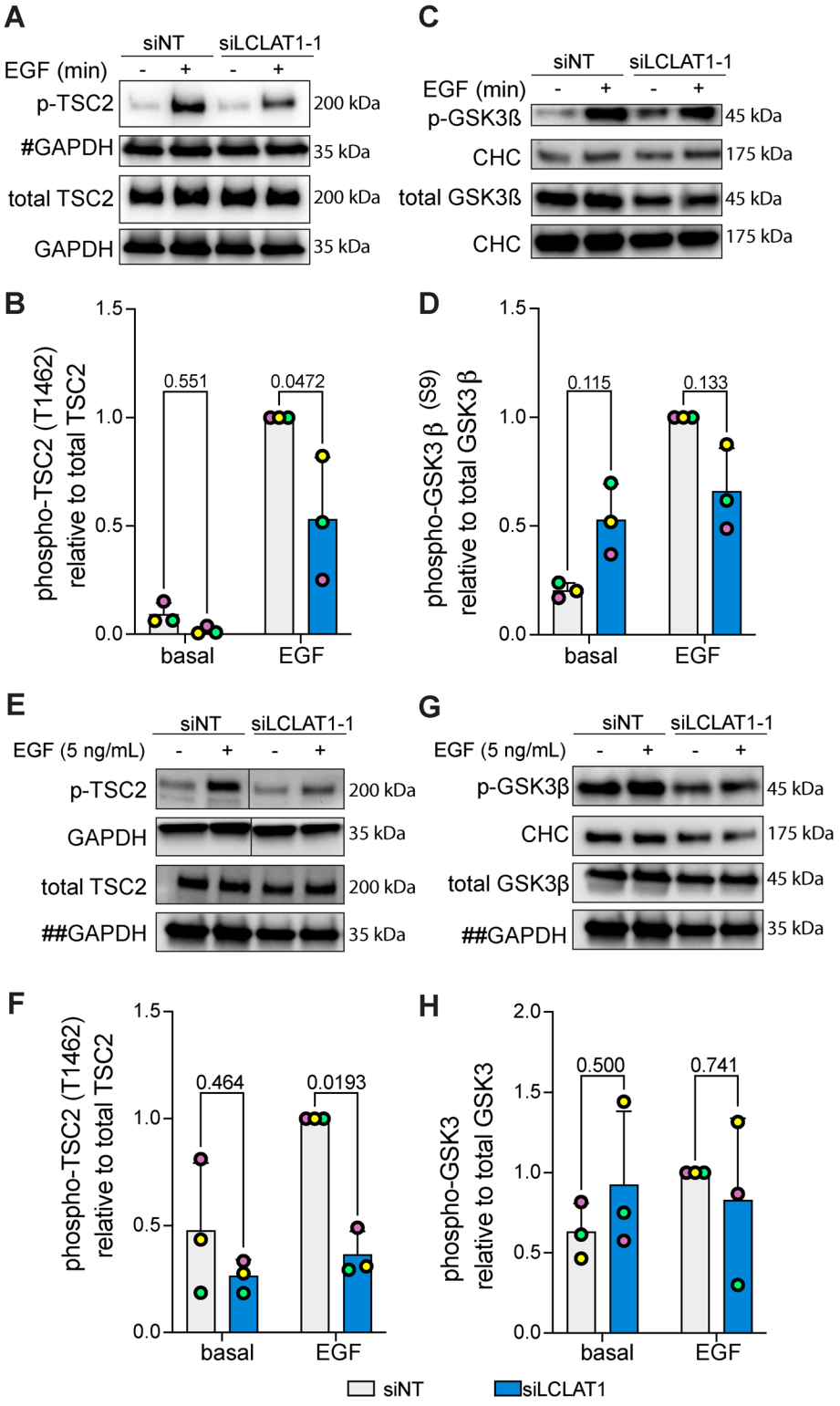

FIGURE 7: LCLAT1 is required for activation of Akt substrates after EGF stimulation. (A, C) Mock-silenced and LCLAT1-silenced ARPE-19 cells were serum-starved (0 min) or stimulated with 5 ng/ml EGF for 5 min. Lysates were then separated by SDS–PAGE and probed by Western blotting for phospho-Tsc2 and total Tsc2 (A) and phospho-GSK3β and total GSK3β (C). Clathrin heavy chain (CHC) or GAPDH were used as loading controls. # indicates that the GAPDH blot was also used as loading control for total pan-Akt in Figure 5A since they originated from the same membrane cut across to probe for different sized proteins. (B, D) Quantification of pTsc2 (B) and pGSK3β (D) normalized to respective total Tsc2 and GSK3β. (E, G) Mock-silenced and LCLAT1-silenced MDA-MB-231 cells were serum-starved (0 min) or stimulated with 5 ng/ml EGF for 5 min. Lysates were then separated by SDS–PAGE and probed by Western blotting for phospho-Tsc2 and total Tsc2 (F), and phospho-GSK3β and total GSK3β (G). Clathrin heavy chain (CHC) or GAPDH were used as loading controls. ## indicates that the GAPDH blot was used as loading control for both total TSC2 (G) and total GSK3β (I) since they originated from the same membrane cut across to probe for different sized proteins. (H, J) Quantification of pTsc2 (H) and pGSK3β (I) normalized to respective total Tsc2 and GSK3β. For B, D, F, and H mean ± STD are shown from $n = 3$ independent experiments. Data points from matching independent experiments are color coded. A two-way ANOVA and Sidak's post-hoc test was used to statistically test the data, with p values shown.

propose at least three possible, nonmutually exclusive mechanisms that will need to be defined in future studies. First, enzymes involved in PtdIns(3,4,5)P_3 metabolism such as class I PI3Ks, the PTEN 3-phosphatase, and the SHIP1/2 5-phosphatase may display acyl sensitivity toward their substrates as previously suggested (Anderson *et al.*, 2016), thus affecting PtdIns(3,4,5)P_3 generation or its turnover. This was observed for type I PIPKs, Vps34 class III PI3Ks, and type II phosphatases (Schmid *et al.*, 2004; Shulga *et al.*, 2012; Ohashi *et al.*, 2020). Second, PtdIns(3,4,5)P_3 levels may be reduced in LCLAT1-disturbed cells due to lower PtdIns(4,5)P_2 substrate levels or availability, which we observed here for MDA-MB-231 cells and previously in ARPE-19 (Bone *et al.*, 2017). This would also be consistent with Wills and colleagues who found that PtdIns(3,4,5)P_3 signaling scales linearly with PtdIns(4,5)P_2 levels during EGF stimulation (Wills *et al.*, 2023). Third, and perhaps linked to the second model above, PtdIns(3,4,5)P_3 synthesis may depend on specific substrate pools. These pools may be highly localized or even channeled through scaffolds (Choi *et al.*, 2016) or transferred at membrane contact sites (Zaman *et al.*, 2020). For example, reduction in PtdIns(4,5)P_2 may lead to impaired clathrin-coated scaffold formation, which promotes EGF-mediated PI3K signaling (Santos *et al.*, 2017; Cabral-Dias *et al.*, 2022). Indeed, we previously showed that LCLAT1 silencing altered clathrin-coated pit dynamics (Bone *et al.*, 2017). Alternatively, contact sites between the endoplasmic reticulum and the plasma membrane are important to generate PtdIns(4,5)P_2 (Chang and Liou, 2015; Kim *et al.*, 2015; Cockcroft *et al.*, 2016; Saheki *et al.*, 2016; Lees *et al.*, 2017; Zaman *et al.*, 2020). These sites may provide precursor pools for PtdIns(4,5)P_2 and/or PtdIns(3,4,5)P_3; consistent with this, depletion of bulk PtdIns(4)P

from the plasma membrane did not reduce PtdIns(4,5)P_2 levels (Hammond *et al.*, 2012), intimating that PtdIns(4,5)P_2 depends on specific pools of PtdIns(4)P. Consistent with this, we previously noted colocalization of a subset of LCLAT1 with proteins known to be at endoplasmic reticulum-plasma membrane contact sites, such as extended synaptotagmins (E-Syt2) (Bone *et al.*, 2017). Thus, LCLAT1 may play a role in generating specific substrate pools to support PtdIns(4,5)P_2 and PtdIns(3,4,5)P_3 at the plasma membrane.

The notion that LCLAT1 may act on specific pools of PtdInsPs is consistent with observations that LCLAT1 and LPIAT/MBOAT7 do not affect the levels of and the acyl profile of all PtdInsPs. For example, their disruption preferentially affects the acyl profile of PtdIns and/or *bis*-phosphorylated PtdInsPs, but not of mono-PtdInsPs in ARPE-19 cells (Anderson *et al.*, 2013; Bone *et al.*, 2017) (Figure 4; Supplemental Figure S3). By comparison, LCLAT1 disruption altered 38:4-PtdIns and 38:4-PtdIns(3,4,5)P_3 in MDA-MB-231 cells, but had little effect on other PtdInsPs in most conditions tested. Thus, LCLAT1 may act on specialized pools of lipids, but this is likely cell-type specific, while enzymes like CDS2 and DGKε may also play a role in establishing PtdInsP acyl profiles (Shulga *et al.*, 2011; D'Souza *et al.*, 2014; Bozelli and Epand, 2019). Overall, while we know that LCLAT1 is needed to boost PtdIns(3,4,5)P_3 levels in response to EGF, the exact mechanism of action remains to be defined.

LCLAT1 and PtdIns(3,4,5)P_3 functions

We witnessed that LCLAT1 supports PtdIns(3,4,5)P_3-mediated activation of Akt isoforms after EGF signaling. Consequently, TSC2 a key target of Akt was less phosphorylated in LCLAT1-silenced cells. Hence, we anticipate that LCLAT1 affects other effector functions of PtdIns(3,4,5)P_3 including activation of other kinases such as Btk and GEFs for the Rho family of GTPases such as Vav1 and Tiam1 (Wang *et al.*, 2006, 2; Salamon and Backer, 2013; Zhu *et al.*, 2015, 1). Additionally, while our work focused on EGFR-mediated signaling, we observed reduced insulin-driven activation of Akt as well (Supplemental Figure S2, D and E). Thus, we postulate that LCLAT1 broadly supports PtdInsP-dependent signaling by other receptor tyrosine kinases, and may also support such signaling by GPCRs and peripherally-associated kinase receptors such as immune receptors (Takeuchi and Ito, 2011; Getahun and Cambier, 2015; Dowling and Mansell, 2016; Bresnick and Backer, 2019). Conceivably, the putative role of LCLAT1 in promoting PI3K signaling among these receptor classes may depend on which isoforms of class I and/or class II PI3K are engaged (Bilanges *et al.*, 2019; Duncan *et al.*, 2020). Overall, our observations establish a key relationship between LCLAT1 and EGFR-PtdIns(3,4,5)P_3-Akt axis and sets a course to determine the universality of LCLAT1 acyltransferase in PtdIns(3,4,5)P_3 signaling. It is important to note that LCLAT1 contribution to signaling likely goes beyond the PI3K pathway. For example, we observed that LCLAT1 silencing by two siRNA oligonucleotides reduced ERK1/2 activation downstream of EGFR in MDA-MB-231 cells, although not in ARPE-19 cells. This distinction between cell lines for ERK1/2 activation is interesting and may speak to the importance of context-dependent signaling since MDA-MB-231 cells carry mutations in KRAS and BRAF genes encoding the K-Ras GTPase and Raf, which control ERK1/2 (Patra *et al.*, 2017; Wagner, 2022). Thus, it may be that these mutations sensitize MDA-MB-231 cells to loss of LCLAT1, although other possibilities remain such as differences between MDA-MB-231 and ARPE-19 cells in their EGFR expression or LCLAT1 silencing efficiency.

LCLAT1 in cellular function and therapeutic potential

While the LCLAT1 acyltransferase remains relatively underinvestigated, LCLAT1 is associated with a variety of functions (Zhang *et al.*, 2023). These include hematopoiesis and cell differentiation (Wang *et al.*, 2007; Xiong *et al.*, 2008; Huang *et al.*, 2014; Huang *et al.*, 2017), metabolic regulation (Cao *et al.*, 2009, 1; Liu *et al.*, 2012), mitochondrial stability, dynamics, and function (Huang *et al.*, 2020; Li *et al.*, 2010, 1; Li *et al.*, 2012), sensitivity to oxidative stress (Li *et al.*, 2010; Liu *et al.*, 2012), endocytosis and endosomal trafficking (Bone *et al.*, 2017), and now receptor tyrosine kinase signaling. LCLAT1 is also proposed to remodel the acyl profile of both cardiolipin and PtdIns/PtdInsPs (Cao *et al.*, 2004, 1; Imae *et al.*, 2012; Li *et al.*, 2010; Bone *et al.*, 2017). It is generally thought that mitochondrial and oxidative stress occurs through cardiolipin remodeling, while endocytosis and receptor signaling is connected to PtdIns acyl function, as proposed here. However, the specific roles of LCLAT1 in cardiolipin and PtdInsP acyl remodeling have not been reconciled. It may be that LCLAT1 has independent roles in acylating these two distinct lipids, or alternatively, one may depend on the other. For example, mitochondria contain PtdIns on their outer membrane, which is important for mitochondria dynamics and function (Pemberton *et al.*, 2020; Zewe *et al.*, 2020). Conceivably, then LCLAT1 acylation of PtdIns may impact lipidomic properties of cardiolipin in mitochondria. In addition, while we did not observe significant changes in Mdm2, p53, and p21 levels that we could specifically attribute to LCLAT1 disturbance, it will be important to examine the effect of LCLAT1 suppression in cell cycle and apoptosis. Unfortunately, we eventually discovered that LCLAT1-1 oligonucleotide appears to have either distinct kinetics of knockdown or a limited set of nonspecific effects on Mdm2 protein levels. Regardless, we have performed extensive experiments that allowed us to ascertain that the effects on PI3K-Akt signaling were observed with multiple LCLAT1 silencing oligonucleotides. Overall, LCLAT1 and its putative partner, MBOAT7/LPIAT1, remain relatively understudied and without well-established inhibitors. Given the role of LCLAT1 in PtdInsP biology and receptor signaling, we propose that these acyltransferases represent new targets for therapeutic development.

MATERIALS AND METHODS

Request a protocol through Bio-protocol.

Cell culture

The male human-derived ARPE-19 retinal pigment epithelial cell line was obtained from ATCC (CRL-2302, Manassas, VA) and was cultured in DMEM/F12 medium (Thermo Fisher Scientific, Mississauga, ON) supplemented with 10% FBS (Wisent, St. Bruno, QB), 100 U/ml penicillin and 100 µg/ml streptomycin (Thermo Fisher Scientific). The female human-derived MDA-MB-231 TNBC cell line was obtained from ATCC (CRM-HTB-26). Wild-type MDA-MB-231 cells and its derivatives (see below) were cultured in DMEM (Wisent) supplemented with 10% FBS, 100 U/ml penicillin, and 100 µg/ml streptomycin. The female human-derived HEK293T cell line was cultured in DMEM with 10% FCS and 1% penicillin/streptomycin. All cells were cultured at 37°C and 5% CO_2. *Mycoplasma* screening is performed at least annually.

Transfection and siRNA-mediated gene silencing

To silence gene expression of LCLAT1 in both ARPE-19 and MDA-MB-231 cells, custom-synthesized siRNA oligonucleotides against LCLAT1 were designed using Horizon Discovery siDESIGN Centre. We designed and tested siLCLAT1-1, siLCLAT1-2, and siLCLAT1-3 with the respective sequences 5′-GGAAAUGGAAGGAUGACAAUU-3′, 5′CAGCAAGUCUCGAAGUAAUU-3′, and 5′-UCGAAGACAUGAUUGAUUAUU-3′. Synthesis was by Sigma-Aldrich (Oakville, ON). In addition, we used siLCLAT1-5, a siGenome-validated

oligonucleotide from Horizon (catalogue no. D-010307-01-0002). Moreover, a nontargeting control siRNA (NT siRNA, or siCON) with the sequence 5′-CGUACUGCUUGCGAUACGGUU-3′ was used (Sigma-Aldrich). Cells were transfected with 22 pmol of siRNA oligonucleotides/well using Lipofectamine RNAiMAX (Thermo Fisher Scientific) in Opti-MEM reduced serum media (Thermo Fisher Scientific) for 3 h at 37°C and 5% CO_2 as per manufacturer's instructions. After transfection, cells were washed and incubated with fresh growth medium. Two rounds of transfection were performed, 72 and 48 h before each experiment.

Plasmids and transfections

Plasmid encoding Akt-PH-GFP was a kind gift from the Balla lab, NIH (Addgene: #51465) and was previously described in (Várnai and Balla, 1998). Akt-PH-GFP plasmid was transfected into ARPE-19 and MDA-MB-231 cells using Lipofectamine 3000 as instructed by the manufacturer. The plasmid encoding eGFP-PLCδ-PH was previously described in (Stauffer *et al*., 1998) and used to generate MDA-MB-231 cells stably expressing the PtdIns(4,5)P_2 biosensor.

Generation of doxycycline-inducible expression of eGFP-PLCδ-PH in MDA-MB-231 cell

A plasmid based on the Sleeping Beauty pSBtet-BP vector (GenScript, Piscataway, NJ; catalogue no.: SC1692) for inducible expression of eGFP-PLCδ1-PH was generated by gene synthesis of the open reading frame of eGFP-PLCδ-PH and insertion into the NheI and ClaI restriction sites of the pSBtet-BP vector, as described previously (Zak and Antonescu, 2023). MDA-MB-231 cells were transfected with the engineered pSBtet-BP::eGFP-PLCδ-PH and pCMV(CAT)T7-SB100 plasmid (Addgene, Plasmid #34879) using FuGENE HD transfection reagent (Promega) as instructed by manufacturer. After transfection, cells were washed and incubated with fresh growth medium for another 24 h to let cells recover in a 6-well plate, and then transferred into a T75 flask in the presence of 3 µg/ml puromycin. Growth medium with puromycin was replaced every 2–3 d for 3 wk. After selection, cells were treated with doxycycline (100-200 nM) for 24 h to detect eGFP-PLCδ-PH expression by Western blotting and fluorescence microscopy.

EGF signaling and Western blotting

Before lysate preparation, cells were incubated with 2 ml of serum free growth medium for 1 h. After serum starvation, cells were stimulated with 5 ng/ml EGF for 5 or 10 min or left unstimulated (basal). Alternatively, cells were stimulated with 10 ng/ml insulin for 5 min. Following serum starvation and subsequent EGF stimulation, whole cell lysates were prepared in 200 µl 2x Laemmli Sample Buffer (0.5 M Tris, pH 6.8, glycerol, and 10% SDS) supplemented with a protease and phosphatase inhibitor cocktail (Complete 1x protease inhibitor (Sigma-Aldrich), 1 mM sodium orthovanadate, and 10 nM okadaic acid). Lysates were heated at 65°C for 15 min and passed through a 27-gauge needle 10 times. Finally, 10% ß-mercaptoethanol and 5% bromophenol blue were added to cell lysates.

Proteins were resolved by Tris-glycine SDS–PAGE and transferred on to a polyvinylidene difluoride (PVDF) membrane. The PVDF membrane was blocked for 1 h at room temperature in blocking buffer composed of 3% BSA in 1X final Tris-buffered saline-Tween (TBS-T; 20 nM Tris, 150 mM NaCl, and 0.1% Tween-20). After blocking, membranes were washed three times with wash buffer and incubated with 1:1000 primary antibody overnight at 4°C. The next day, membranes were washed three times, for 5 min each, and then subjected to 1:1000 secondary antibody for 1 h at room temperature. After incubation with secondary antibody, membranes were washed three times, 5 min each, and imaged using the ChemiDoc Imaging System (Bio-Rad). Membranes were exposed to Immobilon Crescendo Western horseradish peroxidase (HRP) substrate (Millipore Sigma) for 30–60 s and chemiluminescent images were acquired by the ChemiDoc System. Western blot signals were analyzed and quantified using the ImageLab 6.1 (Bio-Rad). Band intensity was obtained by signal integration in an area corresponding to the appropriate band. This value was then normalized to the loading control signal. For quantifying phosphorylated protein levels, the phosphorylated protein signal and the corresponding total protein signal were first normalized to their respective loading controls, followed by the ratio of corrected phosphorylated protein signal to total protein signal.

Primary antibodies raised in rabbit were anti-LCLAT1 (catalogue no. 106759, GeneTex), anti-phospho-Akt (S473, catalogue no. 9271), anti-phospho-Akt1 (S473, catalogue no. 9018), anti-phospho-Akt2 (S474, catalogue no. 8599), anti-Akt1 (catalogue no. 2938), anti-phospho-EGFR (Y1068, catalogue no. 2234), anti-phospho-tuberin/TSC2 (T1462, catalogue no. 3611), anti-tuberin/TSC2 (catalogue no. 3612), anti-phospho-GSK3ß (S9, catalogue no. 9323), anti-phospho-ERK1/2 (T202/Y204, monoclonal, catalogue no. 9201), anti-ERK1/2 (monoclonal, 137F5, catalogue no. 4695), anti-p53 (monoclonal, 7F5, catalogue no. 2527), anti-p21 Waf1/Cip1 (monoclonal, 12D1, catalogue no. 2947), anti-cofilin (monoclonal, D3F9), anti-vinculin (polyclonal, catalogue no. 4550), anti-clathrin, (monoclonal DC36, catalogue no. 4796), and anti-GAPDH (catalogue no. 2118) were all from Cell Signaling Technology. Antibodies raised in mouse were anti-Akt (monoclonal, 40D4; catalogue no. 2920), anti-Akt2 (catalogue no. 5239), anti-GSK3ß (catalogue no. 9832), and anti-puromycin (catalogue no. MABE343) and were all from Cell Signaling Technology. Goat anti-EGFR antibodies were from Santa Cruz Biotechnology (sc-03-G). HRP-linked secondary anti-rabbit, anti-mouse, and anti-goat IgG antibodies were from Cell Signaling Technology.

Fluorescence and immunofluorescence

To detect surface levels of EGFR in MDA-MB-231 and ARPE-19 cells, cells were blocked with 3% BSA in PBS supplemented with 1 mM $CaCl_2$ and $MgCl_2$ for 30 min on ice, followed by 1 h incubation with a 1:200 dilution of mouse anti-EGFR antibody collected in-house from the mAb108 hybridoma obtained from ATCC (Cabral-Dias *et al*., 2022). After washing with PBS, cells were fixed with 4% paraformaldehyde in PBS for 15 min and then quenched with 100 mM glycine in PBS for 10 min, followed by washing with PBS, and then fluorescent secondary mouse antibodies (Jackson ImmunoResearch Labs Inc., West Grove, PA) at a 1:500 dilution in 1% BSA in PBS for 1 h at room temperature. The coverslips were mounted using Dako fluorescence mounting medium (Agilent Technologies, Inc. Mississauga, ON, Canada). For labeling the plasma membrane, cells with stained with 7 µg/ml FM4-64FX and imaged within 10 min to minimize internalization of FM4-64FX.

Microscopy

Confocal and TIRF micrographs were obtained using a Quorum Diskovery spinning disk confocal system coupled to a TIRF module (Quorum Technologies, Inc., Guelph, ON). The microscope itself consisted of an inverted fluorescence microscope (DMi8; Leica) equipped with an Andor Zyla 4.2 Megapixel sCMOS camera (Oxford Instruments, Belfast, UK), a 63x oil immersion objective (1.4 NA), and standard excitation and emission filter sets and lasers were used for all fluorophores. The TIRF module used a 63x/NA1.49 objective with a 1.8x camera relay (total magnification 108x). The microscope

system was controlled by the MetaMorph acquisition software (Molecular Devices, LLC, San Jose, CA, USA).

For fixed cells, z-stacks of 10–30 images were acquired with an interplanal distance of 0.6 µm distance. For live-cell imaging of Akt-PH-GFP dynamics in ARPE-19 cells or of eGFP-PLCδ-PH in MDA-MB-231 cells by TIRF microscopy or spinning disk confocal respectively, cells were maintained in DMEM free of phenol red or serum in a Chamlide microscope-mounted chamber at 37°C and 5% CO_2. For timelapse of Akt-PH-GFP in MDA-MB-231 cells, a baseline was obtained by acquiring images for 1 min at 15 s, then EGF was added, and images acquired every 15 s for 10 min.

Image analysis and processing

Image processing and quantitative analysis were performed using ImageJ or FIJI v. 2.3 (Schindelin *et al.*, 2012) or Volocity v. 7 (Quorum Technologies), where image enhancements were completed without altering the quantitative relationship between image elements. For quantification of EGFR cell surface, regions of interest were generated by freehand to define the cell outline, the mean fluorescence intensity over the whole cell area was calculated, and then background corrected (Cabral-Dias *et al.*, 2022). Mean fluorescence from at least 30 cells per condition per experiment was then normalized against control condition. To obtain the relative cell surface localization index for the Akt-PH-GFP probe in ARPE-19 cells, we used ImageJ to determine the ratio of TIRF/epifluorescence fluorescence for >100 cells per condition per experiment. To measure the plasma membrane to cytosolic ratio of eGFP-PLCδ-PH in MDA-MB-231 cells (Cabral-Dias *et al.*, 2021), we first defined the plasma membrane using the FM4-64FX channel to randomly selected regions of the plasma membrane and cytosol for each cell and their ratio was calculated. For Akt-PH-GFP timelapse movies were acquired and randomly selected regions in the cell periphery and cytosol were selected in FIJI and then the plasma membrane to cytosol fluorescence ratio over time. We examined at least 23 cells over three experiments.

Lipid extraction

Cells were grown to ~0.5×10^6 per well in a 6-well plate. Cells were then placed on ice and the media removed. Cells were scraped in 500 µl of ice-cold 1M HCl and transferred to a precooled safe lock 2 ml microcentrifuge tube. Cells were then collected by centrifugation at 13,000 × *g* for 10 min at 4°C. The supernatant was aspirated, and the pellet was then snap frozen in liquid nitrogen.

Mass spectrometry lipid analysis

Mass spectrometry was used to measure PtdInsPs from lipid extracts prepared from 0.5 to 1×10^6 MDA-MB-231 cells or 0.6×10^6 ARPE-19 cells as described previously (Clark *et al.*, 2011). Briefly, we used a QTRAP 4000 mass spectrometer (A B Sciex, Macclesfield, UK) and employing the lipid extraction and derivatization method described for cultured cells (Clark *et al.*, 2011). The response ratios of a specific PtdInsP acyl species were calculated by normalizing the targeted lipid integrated response area to that of a known amount of added relevant internal standard. A ratio of ratios was then calculated by taking the response ratios of 38:4-PtdIns, 38-4-mono-PtdInsP, 38-4-bis-PtdInsP, and 38:4-PtdIns(3,4,5)P_3 against the sum of response ratios for 36:1 and 36:2 (36:x) of PtdIns or the corresponding 36:x-mono-PtdInsP or 36:x-bis-PtdInsP. Data are presented as mean ± STD from four separate experiments.

Statistical analysis

Experiments were repeated a minimum of three independent times, with the exact number for each experiment indicated in the respective figure legend and/or graph as individual data points. Microscopy data were selected and quantified randomly, that is, before inspection of cells. If regions of a cell were selected, this was done with the independent channel prior to quantification of the target channel. Data were collected as mean ± SD (STD) or ± standard error of the mean (SEM). Statistical comparisons of means were then performed with GraphPad Prism v. 10. Statistical tests were selected based on data conditions such as number of parameters, sample size, assumption of normality, number of comparisons made, and correction for multiple comparisons. Figure legends specify the tests employed for a given dataset such as one-sample *t* test, one-way or repeated-measures two-way ANOVA tests, and recommended post-hoc tests. *p* values are shown, where $p < 0.05$ was typically accepted as significantly different.

ACKNOWLEDGMENTS

We would like to acknowledge funding that made this study possible as follows. RJB and LS are recipients of Canada Research Chairs. RJB was further supported by Toronto Metropolitan University, the Faculty of Science, the Ontario Ministry of Research and Training, the Natural Sciences and Engineering Research Council of Canada, and the Canada Foundation for Innovation. CNA was funded by the Canadian Institutes of Health Research. PH, LS, and KA were funded by the Biotechnology and Biological Sciences Research Council's (BBSRC) Institute Strategic Programmes Grants, LS was funded by the Canadian Institutes of Health.

REFERENCES

Alessi DR, Deak M, Casamayor A, Caudwell FB, Morrice N, Norman DG, Gaffney P, Reese CB, MacDougall CN, Harbison D, *et al.* (1997). 3-Phosphoinositide-dependent protein kinase-1 (PDK1): Structural and functional homology with the Drosophila DSTPK61 kinase. Curr Biol 7, 776–789.

Anderson KE, Kielkowska A, Durrant TN, Juvin V, Clark J, Stephens LR, Hawkins PT (2013). Lysophosphatidylinositol-acyltransferase-1 (LPIAT1) is required to maintain physiological levels of PtdIns and PtdInsP2 in the mouse. PLoS One 8, e58425.

Anderson KE, Juvin V, Clark J, Stephens LR, Hawkins PT (2016). Investigating the effect of arachidonate supplementation on the phosphoinositide content of MCF10a breast epithelial cells. Adv Biol Regul 62, 18–24.

Balla T (2013). Phosphoinositides: Tiny lipids with giant impact on cell regulation. Physiol Rev 93, 1019–1137.

Barneda D, Cosulich S, Stephens L, Hawkins P (2019). How is the acyl chain composition of phosphoinositides created and does it matter? Biochem Soc Trans 47, 1291–1305.

Bellacosa A, Chan TO, Ahmed NN, Datta K, Malstrom S, Stokoe D, McCormick F, Feng J, Tsichlis P (1998). Akt activation by growth factors is a multiple-step process: The role of the PH domain. Oncogene 17, 313–325.

Bilanges B, Posor Y, Vanhaesebroeck B (2019). PI3K isoforms in cell signalling and vesicle trafficking. Nat Rev Mol Cell Biol 20, 515–534.

Blunsom NJ, Cockcroft S (2020). Phosphatidylinositol synthesis at the endoplasmic reticulum. Biochim Biophys Acta Mol Cell Biol Lipids 1865, 158471.

Bone LN, Dayam RM, Lee M, Kono N, Fairn GD, Arai H, Botelho RJ, Antonescu CN (2017). The acyltransferase LYCAT controls specific phosphoinositides and related membrane traffic. Mol Biol Cell 28, 161–172.

Böni-Schnetzler M, Pilch PF (1987). Mechanism of epidermal growth factor receptor autophosphorylation and high-affinity binding. Proc Natl Acad Sci USA 84, 7832–7836.

Bozelli JC, Epand RM (2019). Specificity of acyl chain composition of phosphatidylinositols. Proteomics 19, e1900138.

Bresnick AR, Backer JM (2019). PI3Kβ-A versatile transducer for GPCR, RTK, and small GTPase signaling. Endocrinology 160, 536–555.

Cabral-Dias R, Awadeh Y, Botelho RJ, Antonescu CN (2021). Detection of Plasma Membrane Phosphoinositide Dynamics Using Genetically Encoded Fluorescent Protein Probes. In: Methods in Molecular Biology, 73–89. New York, NY: Humana Press.

Cabral-Dias R, Lucarelli S, Zak K, Rahmani S, Judge G, Abousawan J, DiGiovanni LF, Vural D, Anderson KE, Sugiyama MG, *et al*. (2022). Fyn and TOM1L1 are recruited to clathrin-coated pits and regulate Akt signaling. J Cell Biol 221, e201808181.
Cao J, Liu Y, Lockwood J, Burn P, Shi Y (2004). A novel cardiolipin-remodeling pathway revealed by a gene encoding an endoplasmic reticulum-associated acyl-CoA:lysocardiolipin acyltransferase (ALCAT1) in mouse. J Biol Chem 279, 31727–31734.
Cao J, Shen W, Chang Z, Shi Y (2009). ALCAT1 is a polyglycerophospholipid acyltransferase potently regulated by adenine nucleotide and thyroid status. Am J Physiol Endocrinol Metab 296, E647–E653.
Chang CL, Liou J (2015). Phosphatidylinositol 4, 5-bisphosphate homeostasis regulated by Nir2 and Nir3 proteins at endoplasmic reticulum-plasma membrane junctions. J Biol Chem 290, 14289–14301.
Choi S, Hedman AC, Sayedyahossein S, Thapa N, Sacks DB, Anderson RA (2016). Agonist-stimulated phosphatidylinositol-3,4,5-trisphosphate generation by scaffolded phosphoinositide kinases. Nat Cell Biol 18, 1324–1335.
Choy CH, Han BK, Botelho RJ (2017). Phosphoinositide diversity, distribution, and effector function: Stepping out of the box. Bioessays 39.
Clark J, Anderson KE, Juvin V, Smith TS, Karpe F, Wakelam MJO, Stephens LR, Hawkins PT (2011). Quantification of PtdInsP3 molecular species in cells and tissues by mass spectrometry. Nat Methods 8, 267–272.
Cockcroft S, Garner K, Yadav S, Gomez-Espinoza E, Raghu P (2016). RdgB reciprocally transfers PA and PI at ER-PM contact sites to maintain PI(4,5)P2 homoeostasis during phospholipase C signalling in Drosophila photoreceptors. Biochem Soc Trans 44, 286–292.
Cross DAE, Alessi DR, Cohen P, Andjelkovich M, Hemmings BA (1995). Inhibition of glycogen synthase kinase-3 by insulin mediated by protein kinase B. Nature 378, 785–789.
D Santos RC, Bautista S, Lucarelli S, Bone LN, Dayam RM, Abousawan J, Botelho RJ, Antonescu CN (2017). Selective regulation of clathrin-mediated epidermal growth factor receptor signaling and endocytosis by phospholipase C and calcium. Mol Biol Cell 28, 2802–2818.
Dey N, De P, Leyland-Jones B (2017). PI3K-AKT-mTOR inhibitors in breast cancers: From tumor cell signaling to clinical trials. Pharmacol Ther 175, 91–106.
Dibble CC, Manning BD (2013). Signal integration by mTORC1 coordinates nutrient input with biosynthetic output. Nat Cell Biol 15, 555–564.
Dickson EJ, Hille B (2019). Understanding phosphoinositides: Rare, dynamic, and essential membrane phospholipids. Biochem J 476, 1–23.
Doumane M, Caillaud MC, Jaillais Y (2022). Experimental manipulation of phosphoinositide lipids: from cells to organisms. Trends Cell Biol 32, 445–461.
Dowling JK, Mansell A (2016). Toll-like receptors: The swiss army knife of immunity and vaccine development. Clin Transl Immunology 5, e85.
D'Souza K, Epand RM (2014). Enrichment of phosphatidylinositols with specific acyl chains. Biochim Biophys Acta 1838, 1501–1508.
D'Souza K, Kim YJ, Balla T, Epand RM (2014). Distinct properties of the two isoforms of CDP-diacylglycerol synthase. Biochemistry 53, 7358–7367.
Duncan L, Shay C, Teng Y (2020). PI3K isoform-selective inhibitors in cancer. Adv Exp Med Biol 1255, 165–173.
Freyr Eiriksson F, Kampp Nøhr M, Costa M, Klara Bö dvarsdottir S, Ögmundsdottir HM, Thorsteinsdottir M (2020). Lipidomic study of cell lines reveals differences between breast cancer subtypes. PLoS One 15, e0231289.
Getahun A, Cambier JC (2015). Of ITIMs, ITAMs, and ITAMis: Revisiting immunoglobulin Fc receptor signaling. Immunol Rev 268, 66–73.
Gordon EM, Ravicz JR, Liu S, Chawla SP, Hall FL (2018). Cell cycle checkpoint control: The cyclin G1/Mdm2/p53 axis emerges as a strategic target for broad-spectrum cancer gene therapy - A review of molecular mechanisms for oncologists. Mol Clin Oncol 9, 115–134.
Gullick WJ, Downward J, Waterfield MD (1985). Antibodies to the autophosphorylation sites of the epidermal growth factor receptor protein-tyrosine kinase as probes of structure and function. EMBO J 4, 2869–2877.
Haag M, Schmidt A, Sachsenheimer T, Brügger B (2012). Quantification of signaling lipids by nano-electrospray ionization tandem mass spectrometry (Nano-ESI MS/MS). Metabolites 2, 57–76.
Hammond GRV, Fischer MJ, Anderson KE, Holdich J, Koteci A, Balla T, Irvine RF (2012). PI4P and PI(4,5)P2 are essential but independent lipid determinants of membrane identity. Science 337, 727–730.
Haugh JM, Codazzi F, Teruel M, Meyer T (2000). Spatial sensing in fibroblasts mediated by 3′ phosphoinositides. J Cell Biol 151, 1269–1280.
Hicks AM, DeLong CJ, Thomas MJ, Samuel M, Cui Z (2006). Unique molecular signatures of glycerophospholipid species in different rat tissues analyzed by tandem mass spectrometry. Biochim Biophys Acta 1761, 1022–1029.
Holgado-Madruga M, Emlet DR, Moscatello DK, Godwin AK, Wong AJ (1996). A Grb2-associated docking protein in EGF- and insulin-receptor signalling. Nature 379, 560–564.
Honegger AM, Szapary D, Schmidt A, Lyall R, Van Obberghen E, Dull TJ, Ullrich A, Schlessinger J (1987). A mutant epidermal growth factor receptor with defective protein tyrosine kinase is unable to stimulate proto-oncogene expression and DNA synthesis. Mol Cell Biol 7, 4568–4571.
Hu P, Margolis B, Skolnik EY, Lammers R, Ullrich A, Schlessinger J (1992). Interaction of phosphatidylinositol 3-kinase-associated p85 with epidermal growth factor and platelet-derived growth factor receptors. Mol Cell Biol 12, 981–990.
Huang LS, Mathew B, Li H, Zhao Y, Ma SF, Noth I, Reddy SP, Harijith A, Usatyuk PV, Berdyshev EV, *et al*. (2014). The mitochondrial cardiolipin remodeling enzyme lysocardiolipin acyltransferase is a novel target in pulmonary fibrosis. Am J Respir Crit Care Med 189, 1402–1415.
Huang LS, Jiang P, Feghali-Bostwick C, Reddy SP, Garcia JGN, Natarajan V (2017). Lysocardiolipin acyltransferase regulates TGF-β mediated lung fibroblast differentiation. Free Radic Biol Med 112, 162–173.
Huang LS, Kotha SR, Avasarala S, VanScoyk M, Winn RA, Pennathur A, Yashaswini PS, Bandela M, Salgia R, Tyurina YY, *et al*. (2020). Lysocardiolipin acyltransferase regulates NSCLC cell proliferation and migration by modulating mitochondrial dynamics. J Biol Chem 295, 13393–13406.
Idevall-Hagren O, De Camilli P (2015). Detection and manipulation of phosphoinositides. Biochim Biophys Acta 1851, 736–745.
Imae R, Inoue T, Nakasaki Y, Uchida Y, Ohba Y, Kono N, Nakanishi H, Sasaki T, Mitani S, Arai H (2012). LYCAT, a homologue of *C. elegans acl-8*, *acl-9*, and *acl-10*, determines the fatty acid composition of phosphatidylinositol in mice. J Lipid Res 53, 335–347.
Inoki K, Li Y, Zhu T, Wu J, Guan K-L (2002). TSC2 is phosphorylated and inhibited by Akt and suppresses mTOR signalling. Nat Cell Biol 4, 648–657.
Inoki K, Li Y, Xu T, Guan KL (2003). Rheb GTpase is a direct target of TSC2 GAP activity and regulates mTOR signaling. Genes Dev 17, 1829–1834.
Katan M, Cockcroft S (2020). Phosphatidylinositol(4,5)bisphosphate: diverse functions at the plasma membrane. Essays Biochem 64, 513–531.
Kim YJ, Guzman-Hernandez M-L, Wisniewski E, Balla T (2015). Phosphatidylinositol-phosphatidic acid exchange by Nir2 at ER-PM contact sites maintains phosphoinositide signaling competence. Dev Cell 33, 549–561.
Kiyatkin A, Aksamitiene E, Markevich NI, Borisov NM, Hoek JB, Kholodenko BN (2006). Scaffolding protein Grb2-associated binder 1 sustains epidermal growth factor-induced mitogenic and survival signaling by multiple positive feedback loops. J Biol Chem 281, 19925–19938.
Koizumi A, Narita S, Nakanishi H, Ishikawa M, Eguchi S, Kimura H, Takasuga S, Huang M, Inoue T, Sasaki J, *et al*. (2019). Increased fatty acyl saturation of phosphatidylinositol phosphates in prostate cancer progression. Sci Rep 9, 13257.
Koland JG, Cerione RA (1988). Growth factor control of epidermal growth factor receptor kinase activity via an intramolecular mechanism. J Biol Chem 263, 2230–2237.
Lee H-C, Inoue T, Sasaki J, Kubo T, Matsuda S, Nakasaki Y, Hattori M, Tanaka F, Udagawa O, Kono N, *et al*. (2012). LPIAT1 regulates arachidonic acid content in phosphatidylinositol and is required for cortical lamination in mice. Mol Biol Cell 23, 4689–4700.
Lees JA, Messa M, Sun EW, Wheeler H, Torta F, Wenk MR, De Camilli P, Reinisch KM (2017). Lipid transport by TMEM24 at ER-plasma membrane contacts regulates pulsatile insulin secretion. Science 355, eaah6171.
Li J, Romestaing C, Han X, Li Y, Hao X, Wu Y, Sun C, Liu X, Jefferson LS, Xiong J, *et al*. (2010). Cardiolipin remodeling by ALCAT1 links oxidative stress and mitochondrial dysfunction to obesity. Cell Metab 12, 154–165.
Li J, Liu X, Wang H, Zhang W, Chan DC, Shi Y (2012). Lysocardiolipin acyltransferase 1 (ALCAT1) controls mitochondrial DNA fidelity and biogenesis through modulation of MFN2 expression. Proc Natl Acad Sci USA 109, 6975–6980.
Li S, Shen Y, Wang M, Yang J, Lv M, Li P, Chen Z, Yang J (2017). Loss of PTEN expression in breast cancer: Association with clinicopathological characteristics and prognosis. Oncotarget 8, 32043–32054.

Linggi B, Carpenter G (2006). ErbB receptors: New insights on mechanisms and biology. Trends Cell Biol 16, 649–656.
Liu X, Ye B, Miller S, Yuan H, Zhang H, Tian L, Nie J, Imae R, Arai H, Li Y, *et al*. (2012). Ablation of ALCAT1 mitigates hypertrophic cardiomyopathy through effects on oxidative stress and mitophagy. Mol Cell Biol 32, 4493–4504.
Liu SL, Wang ZG, Hu Y, Xin Y, Singaram I, Gorai S, Zhou X, Shim Y, Min JH, Gong LW, *et al*. (2018). Quantitative lipid imaging reveals a new signaling function of phosphatidylinositol-3,4-bisphophate: Isoform- and site-specific activation of Akt. Mol Cell 71, 1092–1104.e5.
Manning BD, Toker A (2017). AKT/PKB signaling: Navigating the network. Cell 169, 381–405.
Margolis B, Bellot F, Honegger AM, Ullrich A, Schlessinger J, Zilberstein A (1990a). Tyrosine kinase activity is essential for the association of phospholipase C-gamma with the epidermal growth factor receptor. Mol Cell Biol 10, 435–441.
Margolis B, Li N, Koch A, Mohammadi M, Hurwitz DR, Zilberstein A, Ullrich A, Pawson T, Schlessinger J (1990b). The tyrosine phosphorylated carboxyterminus of the EGF receptor is a binding site for GAP and PLC-gamma. EMBO J 9, 4375–4380.
Marshall JG, Booth JW, Stambolic V, Mak T, Balla T, Schreiber AD, Meyer T, Grinstein S (2001). Restricted accumulation of phosphatidylinositol 3-kinase products in a plasmalemmal subdomain during Fc gamma receptor-mediated phagocytosis. J Cell Biol 153, 1369–1380.
Milne SB, Ivanova PT, DeCamp D, Hsueh RC, Brown HA (2005). A targeted mass spectrometric analysis of phosphatidylinositol phosphate species. J Lipid Res 46, 1796–1802.
Morioka S, Nakanishi H, Yamamoto T, Hasegawa J, Tokuda E, Hikita T, Sakihara T, Kugii Y, Oneyama C, Yamazaki M, *et al*. (2022). A mass spectrometric method for in-depth profiling of phosphoinositide regioisomers and their disease-associated regulation. Nat Commun 13, 83.
Mujalli A, Chicanne G, Bertrand-Michel J, Viars F, Stephens L, Hawkins P, Viaud J, Gaits-Iacovoni F, Severin S, Gratacap MP, *et al*. (2018). Profiling of phosphoinositide molecular species in human and mouse platelets identifies new species increasing following stimulation. Biochim Biophys Acta 1863, 1121–1131.
Naguib A, Bencze G, Engle DD, Chio IIC, Herzka T, Watrud K, Bencze S, Tuveson DA, Pappin DJ, Trotman LC (2015). p53 mutations change phosphatidylinositol acyl chain composition. Cell Rep 10, 8–19.
Ohashi Y, Tremel S, Masson GR, McGinney L, Boulanger J, Rostislavleva K, Johnson CM, Niewczas I, Clark J, Williams RL (2020). Membrane characteristics tune activities of endosomal and autophagic human VPS34 complexes. eLife 9, e58281.
Orofiamma LA, Vural D, Antonescu CN (2022). Control of cell metabolism by the epidermal growth factor receptor. Biochim Biophys Acta Mol Cell Res 1869, 119359.
Patra S, Young V, Llewellyn L, Senapati JN, Mathew J (2017). BRAF, KRAS and PIK3CA mutation and sensitivity to trastuzumab in breast cancer cell line model. Asian Pac J Cancer Prev 18, 2209–2213.
Pemberton JG, Kim YJ, Humpolickova J, Eisenreichova A, Sengupta N, Toth DJ, Boura E, Balla T (2020). Defining the subcellular distribution and metabolic channeling of phosphatidylinositol. J Cell Biol 219, e201906130.
Posor Y, Jang W, Haucke V (2022). Phosphoinositides as membrane organizers. Nat Rev Mol Cell Biol 23, 797–816.
Rodgers SJ, Ferguson DT, Mitchell CA, Ooms LM (2017). Regulation of PI3K effector signalling in cancer by the phosphoinositide phosphatases. Biosci Rep 37, BSR20160432.
Rodrigues GA, Falasca M, Zhang Z, Ong SH, Schlessinger J (2000). A novel positive feedback loop mediated by the docking protein Gab1 and phosphatidylinositol 3-kinase in epidermal growth factor receptor signaling. Mol Cell Biol 20, 1448–1459.
Rueda-Rincon N, Bloch K, Derua R, Vyas R, Harms A, Hankemeier T, Ali Khan N, Dehairs J, Bagadi M, Mercedes Binda M, *et al*. (2015). p53 attenuates AKT signaling by modulating membrane phospholipid composition. Oncotarget 6, 21240–21254.
Saheki Y, Bian X, Schauder CM, Sawaki Y, Surma MA, Klose C, Pincet F, Reinisch KM, De Camilli P (2016). Control of plasma membrane lipid homeostasis by the extended synaptotagmins. Nat Cell Biol 18, 504–515.
Salamon RS, Backer JM (2013). Phosphatidylinositol-3,4,5-trisphosphate: Tool of choice for class I PI 3-kinases. Bioessays 35, 602–611.
Schindelin J, Arganda-Carreras I, Frise E, Kaynig V, Longair M, Pietzsch T, Preibisch S, Rueden C, Saalfeld S, Schmid B, *et al*. (2012). Fiji: An open-source platform for biological-image analysis. Nat Methods 9, 676–682.
Schmid AC, Wise HM, Mitchell CA, Nussbaum R, Woscholski R (2004). Type II phosphoinositide 5-phosphatases have unique sensitivities towards fatty acid composition and head group phosphorylation. FEBS Lett 576, 9–13.
Shulga YV, Topham MK, Epand RM (2011). Substrate specificity of diacylglycerol kinase-epsilon and the phosphatidylinositol cycle. FEBS Lett 585, 4025–4028.
Shulga YV, Anderson RA, Topham MK, Epand RM (2012). Phosphatidylinositol-4-phosphate 5-kinase isoforms exhibit acyl chain selectivity for both substrate and lipid activator. J Biol Chem 287, 35953–35963.
Stauffer TP, Ahn S, Meyer T (1998). Receptor-induced transient reduction in plasma membrane PtdIns(4,5)P2 concentration monitored in living cells. Curr Biol 8, 343–346.
Stokoe D, Stephens LR, Copeland T, Gaffney PRJ, Reese CB, Painter GF, Holmes AB, McCormick F, Hawkins PT (1997). Dual role of phosphatidylinositol-3,4,5-trisphosphate in the activation of protein kinase B. Science 277, 567–570.
Sugiyama MG, Fairn GD, Antonescu CN (2019). Akt-ing up just about everywhere: Compartment-specific Akt activation and function in receptor tyrosine kinase signaling. Front Cell Dev Biol 7, 70.
Sun Y, Thapa N, Hedman AC, Anderson RA (2013). Phosphatidylinositol 4,5-bisphosphate: targeted production and signaling. Bioessays 35, 513–522.
Takeuchi K, Ito F (2011). Receptor tyrosine kinases and targeted cancer therapeutics. Biol Pharm Bull 34, 1774–1780.
Traynor-Kaplan A, Kruse M, Dickson EJ, Dai G, Vivas O, Yu H, Whittington D, Hille B (2017). Fatty-acyl chain profiles of cellular phosphoinositides. Biochim Biophys Acta 1862, 513–522.
Várnai P, Balla T (1998). Visualization of phosphoinositides that bind pleckstrin homology domains: Calcium- and agonist-induced dynamic changes and relationship to myo-[3H]inositol-labeled phosphoinositide pools. J Cell Biol 143, 501–510.
Wagner K-U (2022). Know thy cells: commonly used triple-negative human breast cancer cell lines carry mutations in RAS and effectors. Breast Cancer Res 24, 44.
Wang SE, Shin I, Wu FY, Friedman DB, Arteaga CL (2006). HER2/Neu (ErbB2) signaling to Rac1-Pak1 is temporally and spatially modulated by transforming growth factor beta. Cancer Res 66, 9591–9600.
Wang C, Faloon PW, Tan Z, Lv Y, Zhang P, Ge Y, Deng H, Xiong JW (2007). Mouse lysocardiolipin acyltransferase controls the development of hematopoietic and endothelial lineages during in vitro embryonic stem-cell differentiation. Blood 110, 3601–3609.
Wills RC, Doyle CP, Zewe JP, Pacheco J, Hansen SD, Hammond GRV (2023). A novel homeostatic mechanism tunes PI(4,5)P2-dependent signaling at the plasma membrane. J Cell Sci 136, jcs261494.
Xiong JW, Yu Q, Zhang J, Mably JD (2008). An acyltransferase controls the generation of hematopoietic and endothelial lineages in zebrafish. Circ Res 102, 1057–1064.
Yarden Y, Schlessinger J (1987). Epidermal growth factor induces rapid, reversible aggregation of the purified epidermal growth factor receptor. Biochemistry 26, 1443–1451.
Zak K, Antonescu CN (2023). Doxycycline-inducible expression of proteins at near-endogenous levels in mammalian cells using the sleeping beauty transposon system. Bio Protoc 13, e4846.
Zaman MF, Nenadic A, Radojičić A, Rosado A, Beh CT (2020). Sticking with it: ER-PM membrane contact sites as a coordinating nexus for regulating lipids and proteins at the cell cortex. Front Cell Dev Biol 8, 675.
Zewe JP, Miller AM, Sangappa S, Wills RC, Goulden BD, Hammond GRV (2020). Probing the subcellular distribution of phosphatidylinositol reveals a surprising lack at the plasma membrane. J Cell Biol 219, e201906127.
Zhang K, Chan V, Botelho RJ, Antonescu CN (2023). A tail of their own: regulation of cardiolipin and phosphatidylinositol fatty acyl profile by the acyltransferase LCLAT1. Biochem Soc Trans 51, 1765–1776.
Zhu G, Fan Z, Ding M, Zhang H, Mu L, Ding Y, Zhang Y, Jia B, Chen L, Chang Z, *et al*. (2015). An EGFR/PI3K/AKT axis promotes accumulation of the Rac1-GEF Tiam1 that is critical in EGFR-driven tumorigenesis. Oncogene 34, 5971–5982.